JAEA-Data/Code
2013-021

Heat Transfer from Fuel Rod Surface under Reactivity-initiated Accident Conditions

- NSRR Experiments under Varied Cooling Conditions -

Yutaka UDAGAWA, Tomoyuki SUGIYAMA and Masaki AMAYA

Reactor Safety Research Unit
Nuclear Safety Research Center

February 2014

Japan Atomic Energy Agency

日本原子力研究開発機構

JAEA-Data/Code

本レポートは独立行政法人日本原子力研究開発機構が不定期に発行する成果報告書です。
本レポートの入手並びに著作権利用に関するお問い合わせは、下記あてにお問い合わせ下さい。
なお、本レポートの全文は日本原子力研究開発機構ホームページ（http://www.jaea.go.jp）
より発信されています。

独立行政法人日本原子力研究開発機構　研究技術情報部　研究技術情報課
〒319-1195　茨城県那珂郡東海村白方白根 2 番地 4
電話 029-282-6387, Fax 029-282-5920, E-mail:ird-support@jaea.go.jp

This report is issued irregularly by Japan Atomic Energy Agency.
Inquiries about availability and/or copyright of this report should be addressed to
Intellectual Resources Section, Intellectual Resources Department,
Japan Atomic Energy Agency.
2-4 Shirakata Shirane, Tokai-mura, Naka-gun, Ibaraki-ken 319-1195 Japan
Tel +81-29-282-6387, Fax +81-29-282-5920, E-mail:ird-support@jaea.go.jp

JAEA-Data/Code 2013-021

Heat Transfer from Fuel Rod Surface under Reactivity-initiated Accident Conditions - NSRR Experiments under Varied Cooling Conditions -

Yutaka UDAGAWA, Tomoyuki SUGIYAMA and Masaki AMAYA

Reactor Safety Research Unit
Nuclear Safety Research Center
Japan Atomic Energy Agency
Tokai-mura, Naka-gun, Ibaraki-ken

(Received November 19, 2013)

The temperature evolution of fuel cladding during a reactivity-initiated accident (RIA) involves rapid changes in the mechanical properties of the cladding tube and is believed to play the primary role in fuel behaviors such as deformation and failure. Cladding-temperature behavior accompanied by boiling of coolant water, which is the case of an RIA in light-water reactors, is influenced by cooling conditions such as subcooling, pressure, and flow velocity. In order to study the effects of cooling conditions on the boiling heat transfer from the fuel rod surface to the coolant water, RIA-simulating experiments with fresh fuels had been conducted in the nuclear safety research reactor (NSRR) under cooling conditions with subcoolings of ~10 to 80 K, flow velocities of 0 to ~3 m/s, pressures of 0.1 to ~16 MPa. In addition, pre-irradiated fuels had been subjected to the NSRR experiments under cooling conditions with subcoolings of ~80 K, stagnant water, and atmospheric pressure. Out of the NSRR experiments, this report presents the fuel specifications, the test conditions, and the transient records during the pulse operations for the cases that the cladding temperature had been successfully measured. Characteristic parameters such as cladding peak temperatures were extracted from the transient records for summarizing the effects of cooling conditions and pre-irradiation on the heat transfer from the cladding surface.

Keywords: LWR Fuel, RIA, NSRR, CHF, Transient Boiling, Film Boiling

JAEA-Data/Code 2013-021

反応度事故時の被覆管表面伝熱挙動
―冷却条件をパラメータとしたNSRR実験―

日本原子力研究開発機構
安全研究センター 原子炉安全研究ユニット
宇田川　豊、杉山　智之、天谷　政樹

(2013年11月19日　受理)

軽水炉の反応度事故において、燃料ペレット温度の上昇に伴って生じる被覆管温度の上昇は、燃料の変形及び破損挙動を決定づける因子の一つとなる。冷却水の沸騰を伴う被覆管表面の伝熱挙動は、冷却水の圧力、サブクール度、流速等の影響を受けることから、これらのパラメータが反応度事故条件下の被覆管表面伝熱挙動に及ぼす影響を調べるため、大気圧から約16MPaの圧力、約10から80 Kのサブクール度、静止水から約3 m/sまでの流動水等、広範な冷却水条件にわたる反応度事故模擬実験が、原子炉安全性研究炉（NSRR）において実施された。また室温大気圧条件については、試験炉で予備照射された燃料についてもNSRR実験が行われ、データが取得されている。本報告は、反応度事故条件下における被覆管の伝熱挙動に関するデータ及び知見の取得を目的として行われたNSRR実験の内、有効な被覆管温度データの取得に成功した実験ケースについて、これまでに公開されていないケースを含め体系的にとりまとめ、冷却水の圧力、サブクール、流速、予備照射の有無等諸パラメータの効果について整理したものである。

原子力科学研究所（駐在）：〒319-1195　茨城県那珂郡東海村白方白根2-4

Contents

1. Introduction ---- 1
2. Experimental ---- 2
2.1 NSRR Facility ---- 2
2.2 Test Capsules ---- 2
2.3 Test Fuel Rod ---- 3
2.4 Instrumentation and Data Acquisition ---- 3
2.5 Data List for Analysis ---- 4
3. Analysis of Experimental Results ---- 6
3.1 Characteristic Parameters for Cladding Temperature Behavior ---- 6
3.2 Evaluation of Fuel Enthalpy ---- 6
3.3 Treatment of Iterative Pulse-irradiation Experiment Results ---- 7
3.4 Effect of Coolant Subcooling ---- 7
3.5 Effect of Coolant Pressure ---- 8
3.6 Effect of Coolant Flow Velocity ---- 9
3.7 Effect of Cladding Pre-irradiation ---- 9
4. Summary ---- 11
Acknowledgements ---- 11
References ---- 11
Appendix CD-ROM
Appendix 1 NSRR Transient Records (Fresh Fuel Tests)
Appendix 2 NSRR Transient Records (JMTR Pre-irradiated Fuel Tests)

目　次

1. 序言 ---- 1
2. 実験 ---- 2
2.1 NSRR 施設 ---- 2
2.2 実験カプセル ---- 2
2.3 実験燃料棒 ---- 3
2.4 計装及びデータ収録 ---- 3
2.5 分析に用いたデータ ---- 4
3. 実験結果の分析 ---- 6
3.1 被覆管温度挙動の特性パラメータ ---- 6
3.2 燃料エンタルピの評価 ---- 6
3.3 繰返し照射実験結果の取扱い ---- 7
3.4 冷却材サブクール度の効果 ---- 7
3.5 冷却材圧力の効果 ---- 8
3.6 冷却材流速の効果 ---- 9
3.7 被覆管予備照射の効果 ---- 9
4. 結言 ---- 11
謝辞 ---- 11
参考文献 ---- 11
付録 CD
付録 1　NSRR 実験過渡記録（未照射燃料実験）
付録 2　NSRR 実験過渡記録（JMTR 予備照射燃料実験）

Figure list

Fig.2.1 Typical histories of NSRR power and time-integrated NSRR power in RIA test ---- 13
Fig.2.2 Outline of NSRR ---- 13
Fig.2.3 Capsule for fresh fuel test at room temperature and atmospheric pressure ---- 14
Fig.2.4 Capsules for fresh fuel test at high temperature and high pressure ---- 14
Fig.2.5 Capsules for JMTR pre-irradiated fuel test ---- 15
Fig.2.6 Design of NSRR standard test fuel rod for fresh fuel test ---- 16
Fig.2.7 Design of JMTR pre-irradiated fuel rod ---- 16
Fig.2.8 Thermocouple attachment on the cladding surface ---- 17
Fig.3.1 Peak temperatures for test cases with fresh fuel, stagnant coolant, atmospheric coolant pressure, and coolant subcoolings of ~10–80 K ---- 18
Fig.3.2 Peak temperatures for test cases with fresh fuel, coolant flow velocity of ~1.0 m/s, atmospheric coolant pressure, and coolant subcoolings of ~20–80 K ---- 18
Fig.3.3 Peak temperatures for test cases with fresh fuel, coolant flow velocity of ~1.8 m/s, atmospheric coolant pressure, and coolant subcoolings of ~20–80 K ---- 19
Fig.3.4 Peak temperatures for test cases with fresh fuel, stagnant coolant, coolant pressure of ~7 MPa, and coolant subcoolings of ~10–230 K ---- 19
Fig.3.5 Peak temperatures for test cases with fresh fuel, stagnant coolant, coolant pressures of ~13–16 MPa, and coolant subcoolings of ~20–50 K ----20
Fig.3.6 Peak temperatures for test cases with fresh fuel, coolant flow velocity of ~1.0 m/s, coolant pressure of ~7 MPa, and coolant subcoolings of ~10–60 K ---- 20
Fig.3.7 Film boiling times for test cases with fresh fuel, stagnant coolant, atmospheric coolant pressure, and coolant subcoolings of ~10–80 K ---- 21
Fig.3.8 Film boiling times for test cases with fresh fuel, coolant flow velocity of ~1.0 m/s, atmospheric coolant pressure, and coolant subcoolings of ~20–80 K ---- 21
Fig.3.9 Film boiling times for test cases with fresh fuel, coolant flow velocity of ~1.8 m/s, atmospheric coolant pressure, and coolant subcoolings of ~20–80 K ---- 22
Fig.3.10 Film boiling times for test cases with fresh fuel, stagnant coolant, coolant pressure of ~7 MPa, and coolant subcoolings of ~10–230 K ---- 22

Fig.3.11 Film boiling times for test cases with fresh fuel, stagnant coolant, coolant pressures of ~13–16 MPa, and coolant subcoolings of ~20–50 K ----- 23
Fig.3.12 Film boiling times for test cases with fresh fuel, coolant flow velocity of ~1.0 m/s, coolant pressure of ~7 MPa, and coolant subcoolings of ~10–60 K ----- 23
Fig.3.13 Surface superheats at quench for test cases with fresh fuel, stagnant coolant, atmospheric coolant pressure, and coolant subcoolings of ~10–80 K ----- 24
Fig.3.14 Surface superheats at quench for test cases with fresh fuel, coolant flow velocity of ~1.0 m/s, atmospheric coolant pressure, and coolant subcoolings of ~20–80 K ----- 24
Fig.3.15 Surface superheats at quench for test cases with fresh fuel, coolant flow velocity of ~1.8 m/s, atmospheric coolant pressure, and coolant subcoolings of ~20–80 K ----- 25
Fig.3.16 Surface superheats at quench for test cases with fresh fuel, stagnant coolant, coolant pressure of ~7 MPa, and coolant subcoolings of ~10–230 K ----- 25
Fig.3.17 Surface superheats at quench for test cases with fresh fuel, coolant flow velocity of ~1.0 m/s, coolant pressure of ~7 MPa, and coolant subcoolings of ~10–60 K ----- 26
Fig.3.18 Peak temperatures for test cases with fresh fuel, stagnant coolant, coolant pressures of ~0.1–7 MPa, and coolant subcooling of ~10 K ----- 26
Fig.3.19 Peak temperatures for test cases with fresh fuel, stagnant coolant, coolant pressures of ~7–15 MPa, and coolant subcoolings of ~20–30 K ----- 27
Fig.3.20 Peak temperatures for test cases with fresh fuel, stagnant coolant, coolant pressures of ~0.1–7 MPa, and coolant subcooling of ~80 K ----- 27
Fig.3.21 Peak temperatures for test cases with fresh fuel, coolant flow velocities of ~0.6–0.7 m/s, coolant pressures of ~0.1–7 MPa, and coolant subcooling of ~20 K ----- 28
Fig.3.22 Peak temperatures for test cases with fresh fuel, coolant flow velocity of ~1.0 m/s, coolant pressures of ~0.1–16 MPa, and coolant subcooling of ~40 K ----- 28
Fig.3.23 Peak temperatures for test cases with fresh fuel, coolant flow velocity of ~1.0 m/s, coolant pressures of ~0.1–16 MPa, and coolant subcoolings of ~50–80 K ----- 29
Fig.3.24 Film boiling times for test cases with fresh fuel, stagnant coolant, coolant pressures of ~0.1–7 MPa, and coolant subcoolings of ~10 K ----- 29

Fig.3.25 Film boiling times for test cases with fresh fuel, stagnant coolant, coolant pressures of ~7–15 MPa, and coolant subcoolings of ~20–30 K ------- 30
Fig.3.26 Film boiling times for test cases with fresh fuel, stagnant coolant, coolant pressures of ~0.1–7 MPa, and coolant subcooling of ~80 K ---------- 30
Fig.3.27 Film boiling times for test cases with fresh fuel, coolant flow velocities of ~0.6–0.7 m/s, coolant pressures of ~0.1–7 MPa, and coolant subcooling of ~20 K ---------- 31
Fig.3.28 Film boiling times for test cases with fresh fuel, coolant flow velocity of ~1.0 m/s, coolant pressures of ~0.1–16 MPa, and coolant subcooling of ~40 K ---------- 31
Fig.3.29 Film boiling times for test cases with fresh fuel, coolant flow velocity of ~1.0 m/s, coolant pressures of ~0.1–16 MPa, and coolant subcoolings of ~50–80 K ---------- 32
Fig.3.30 Surface superheats at quench for test cases with fresh fuel, stagnant coolant, coolant pressures of ~0.1–7 MPa, and coolant subcoolings of ~10 K ---------- 32
Fig.3.31 Film boiling times for test cases with fresh fuel, stagnant coolant, coolant pressures of ~7–15 MPa, and coolant subcoolings of ~20–30 K ------- 33
Fig.3.32 Surface superheats at quench for test cases with fresh fuel, stagnant coolant, coolant pressures of ~0.1–7 MPa, and coolant subcooling of ~80 K ---------- 33
Fig.3.33 Surface superheats at quench for test cases with fresh fuel, coolant flow velocities of ~0.6–0.7 m/s, coolant pressures of ~0.1–7 MPa, and coolant subcooling of ~20 K ---------- 34
Fig.3.34 Surface superheats at quench for test cases with fresh fuel, coolant flow velocity of ~1.0 m/s, coolant pressures of ~0.1–16 MPa, and coolant subcooling of ~40 K ---------- 34
Fig.3.35 Surface superheats at quench for test cases with fresh fuel, coolant flow velocity of ~1.0 m/s, coolant pressures of ~0.1–16 MPa, and coolant subcoolings of ~50–80 K ---------- 35
Fig.3.36 Peak temperatures for test cases with fresh fuel, coolant flow velocities of ~0.6–1.8 m/s, atmospheric coolant pressure, and coolant subcooling of ~20 K ---------- 35
Fig.3.37 Peak temperatures for test cases with fresh fuel, coolant flow velocities of ~0.0–3.2 m/s, atmospheric coolant pressure, and coolant subcooling of ~80 K ---------- 36

Fig.3.38 Peak temperatures for test cases with fresh fuel, coolant flow velocities of ~0.0–3.0 m/s, coolant pressure of ~7 MPa, and coolant subcooling of ~10 K ---- 36
Fig.3.39 Peak temperatures for test cases with fresh fuel, coolant flow velocities of ~0.0–3.0 m/s, coolant pressure of ~7 MPa, and coolant subcoolings of ~10–30 K ---- 37
Fig.3.40 Peak temperatures for test cases with fresh fuel, coolant flow velocities of ~0.0–1.0 m/s, coolant pressures of ~12–16 MPa, and coolant subcoolings of ~40–50 K ---- 37
Fig.3.41 Film boiling times for test cases with fresh fuel, coolant flow velocities of ~0.6–1.8 m/s, atmospheric coolant pressure, and coolant subcooling of ~20 K ---- 38
Fig.3.42 Film boiling times for test cases with fresh fuel, coolant flow velocities of ~0.0–3.2 m/s, atmospheric coolant pressure, and coolant subcooling of ~80 K ---- 38
Fig.3.43 Film boiling times for test cases with fresh fuel, coolant flow velocities of ~0.0–3.0 m/s, coolant pressure of ~7 MPa, and coolant subcooling of ~10 K ---- 39
Fig.3.44 Film boiling times for test cases with fresh fuel, coolant flow velocities of ~0.0–3.0 m/s, coolant pressure of ~7 MPa, and coolant subcoolings of ~10–30 K ---- 39
Fig.3.45 Film boiling times for test cases with fresh fuel, coolant flow velocities of ~0.0–1.0 m/s, coolant pressures of ~12–16 MPa, and coolant subcoolings of ~40–50 K ---- 40
Fig.3.46 Surface superheats at quench for test cases with fresh fuel, coolant flow velocities of ~0.6–1.8 m/s, atmospheric coolant pressure, and coolant subcooling of ~20 K ---- 40
Fig.3.47 Surface superheats at quench for test cases with fresh fuel, coolant flow velocities of ~0.0–3.2 m/s, atmospheric coolant pressure, and coolant subcooling of ~80 K ---- 41
Fig.3.48 Surface superheats at quench for test cases with fresh fuel, coolant flow velocities of ~0.0–3.0 m/s, coolant pressure of ~7 MPa, and coolant subcooling of ~10 K ---- 41
Fig.3.49 Surface superheats at quench for test cases with fresh fuel, coolant flow velocities of ~0.0–3.0 m/s, coolant pressure of ~7 MPa, and coolant subcoolings of ~10–30 K ---- 42

Fig.3.50 Peak temperatures for test cases with fresh and irradiated fuels, stagnant coolant, atmospheric coolant pressure, and coolant subcooling of ~80 K ---------- 42
Fig.3.51 Film boiling times for test cases with fresh and irradiated fuels, stagnant coolant, atmospheric coolant pressure, and coolant subcooling of ~80 K ---------- 43
Fig.3.52 Surface superheats at quench for test cases with fresh and irradiated fuels, stagnant coolant, atmospheric coolant pressure, and coolant subcooling of ~80 K ---------- 43

This is a blank page.

1. Introduction

The temperature evolution of fuel cladding during a reactivity-initiated accident (RIA) involves rapid changes in the mechanical properties of the cladding tube and is believed to play the primary role in fuel behaviors such as deformation and failure. Cladding-temperature behavior accompanied by boiling of coolant water, which is the case of an RIA in light-water reactors and known as "Departure from Nucleate Boiling (DNB)", is influenced by coolant conditions such as subcooling, pressure, and flow velocity.

To study the effects of the coolant conditions on the boiling heat transfer from the fuel rod surface to the coolant water has been therefore one of the main purposes of RIA research programs of Japan Atomic Energy Agency (JAEA), and so RIA-simulating experiments with fresh fuels had been conducted in the nuclear safety research reactor (NSRR) under a wide range of coolant conditions: subcoolings of ~10 to 80 K, flow velocities of 0 to ~3 m/s, and pressures of 0.1 to ~16 MPa. Also pre-irradiated fuels had been subjected to the NSRR experiments under coolant conditions with subcoolings of ~10 to 80 K, stagnant water, and pressures of 0.1 to ~7 MPa.

Ohnishi et al. proposed an empirical model for the boiling heat transfer during an RIA on the basis of their investigation on a part of the results of the NSRR experiments.[1)] But their model was not well validated for the forced flow coolant conditions, since the corresponding data from the NSRR experiments were not fully available at that time. Up to the present time none of existing computer codes for transient fuel behavior has not been verified with temperature data measured under the varied conditions of coolant and fuel rods, to our knowledge.

The purpose of the present publication is to provide an open access to the forementioned NSRR-experiment data, which are useful for the model validation, since a considerable part of the data have remained undisclosed. Out of the experiments, this report presents the fuel specifications, the test conditions, and the transient records during the pulse operations for the cases that the cladding temperature had been successfully measured. Characteristic parameters such as cladding peak temperatures were extracted from the transient records for summarizing the effects of coolant conditions and pre-irradiation on the heat transfer from the fuel-rod surface to the coolant water.

2. Experimental

2.1 NSRR Facility

The NSRR is a modified TRIGA Annular Core Pulse Reactor (ACPR). The TRIGA type reactor is known for the unique nature of a negative reactivity coefficient provided by the uranium zirconium hydride (UZrH) fuel. The NSRR is a modified type with an enhanced negative feedback nature which enables the reactor to produce a high power pulse reaching approximately 23 GW. Fig.2.1 shows typical histories of the power and time-integrated power of the NSRR. RIA-simulation tests have been performed by using this pulse-operation capability since the construction in 1975. Another main feature of the NSRR is the large experimental cavity at the core center as shown in Fig.2.2, which enables loading of a test capsule with a diameter up to 200 mm. This permits flexible design of the test capsule and simulation of broad range of accident conditions.

Details of the NSRR facility and early results are described in references. [2, 3)]

2.2 Test Capsules

Atmospheric pressure capsule for fresh fuel test

Fig.2.3 shows the NSRR atmospheric pressure capsule for fresh fuel tests. The capsule is made of the stainless steel and has air- and pressure-tightness enough to confine radioactive materials which can be released in case of fuel rod failure during the test. The coolant water condition is normally stagnant at room temperature (approximately 293 K) and atmospheric pressure (0.1 MPa). The water temperature can be raised up to ~363 K (~10 K below the boiling temperature at 0.1 MPa) by using an electric heater. Flow condition can be achieved by using a capsule internal pump and fuel shroud.

High temperature and high pressure capsules for fresh fuel test

Fig.2.4 shows the high temperature and high pressure (HTHP) capsules. The left one in the figure is the stagnant coolant type with a capsule internal heater. [4)] The right one is the loop type capsule which is connected with an external coolant loop system with a heater, pressurizer and pump. [5)]

Atmospheric pressure capsule for JMTR pre-irradiated fuel test

Fig.2.5 shows the atmospheric pressure capsule for the pre-irradiated fuels [6)] in the Japan Materials Testing Reactor (JMTR). Functions are the same as those of the atmospheric capsule for fresh fuel test, but this capsule consists of double containers to enhance confinement performance for the fuel and fission products with high radioactivity. The capsule internal pump is not available because of the spatial limit.

2.3 Test Fuel Rod

The NSRR test fuel rod is normally about 300 mm in total length. Fig.2.6 shows the design of NSRR standard test fuel rod for fresh fuel test. The specifications of pellet and cladding are those of the PWR 14x14 fuel rod. The cladding material is Zircaloy-4. The U-235 enrichment of fuel pellets are 10%, and typically lower enriched pellets are placed at the top and bottom ends of the pellet stack to avoid the end power peaking. The fuel rod design can vary with the test objectives; the U-235 enrichment, length of pellet stack, cladding material, cladding geometry, pellet-cladding gap, fill-gas composition and pressure, cladding surface pre-oxidation, and so on.

Fig.2.7 shows the design of JMTR pre-irradiated fuel rod which is similar to the design of fresh fuel test rod.

2.4 Instrumentation and Data Acquisition

This report focuses on the cladding surface heat transfer. Therefore, the most important instrumentation is the cladding surface thermocouples (TCs). Normally, bare wires of the type R (Pt-13%Rh vs. Pt) TC are directly welded on the cladding surface to form intrinsic junctions as illustrated in Fig.2.8. The TC wire diameter is 0.2 or 0.3 mm, depending on the tests. As the cladding surface TC is not connected to the compensation wire, it measures the temperature difference between the cladding surface and the junction between the TC wire and lead wire, which is ~30mm away from the cladding surface in the coolant water. Therefore, the measured temperature must be corrected by considering the coolant temperature. In some tests, pellet center temperature was measured with the sheathed tungsten-rhenium (W-5%Re vs. W-26%Re) TC. In addition to TCs, strain gauge type pressure sensors, LVDT (linear variable differential transformer) elongation sensors for pellet stack and cladding, and other sensors are used depending on the test objective.

In order to minimize the possible delay in TC response, TC wires with small diameters were used for the cladding surface temperature measurement. On the other hand, there could be discernible delay in the output from the sheathed TCs. In addition, there are other factors reducing the temperature measurement accuracy, such as the fin effect by TCs and the gamma-heating in the attached materials and in the TC element itself. As for the pressure measurement, since the strain gauge nature is strongly affected by the gamma field, the pressure measurement accuracy during the pulse power is degraded. It must be noted that the transient records provided in the appendices of this report are raw data without any correction, because of the difficulty of reliable correction. However, discussions on the cladding surface temperature during the stable film boiling are based on the corrected temperature considering the TC fin effect (to be discussed in chapter 3).

The signals from all sensors in the test capsule are amplified and sent to the data acquisition system. The acquisition system used high-speed analog recorder using a multitrack magnetic tape, and the analog-to-digital conversion was performed after the tests. Most of the transient records presented in the appendices of this report were acquired with this system. The recorder was replaced with a digital recorder with real-time A/D conversion capability in 1999. In this report, only the data of 562 test series were acquired with the digital system.

2.5 Data List for Analysis

The identification numbers of the NSRR tests, for which data analysis will be performed in the chapter 3, are listed below. All the transient records in these tests are provided in the appendices.

Fresh fuel tests:

Tests with atmospheric pressure capsule

Test 103-2	Test 240-2	Test 240-17-2	Test 562-1
Test 103-7	Test 240-3	Test 241-1	Test 562-2
Test 103-23	Test 240-4	Test 241-3	Test 562-3
Test 103-24	Test 240-5	Test 241-5	Test 562-4
Test 103-31-1	Test 240-6	Test 241-5B	Test 562-5
Test 103-31-2	Test 240-7	Test 242-1	Test 562-6
Test 103-31-3	Test 240-8	Test 242-2	Test 562-7
Test 103-32	Test 240-9	Test 242-3	Test 562-8
Test 105-2-1	Test 240-10	Test 242-4	Test 562-9
Test 206-14	Test 240-12	Test 252-5	Test 562-10
Test 206-34	Test 240-13-1	Test 252-8	Test 562-11
Test 206-39	Test 240-13-2	Test 253-3	Test 562-12
Test 206-40	Test 240-13-3	Test 253-6	Test 562-13
Test 234-7	Test 240-14-1	Test 253-10	Test 562-14
Test 240-1	Test 240-14-2	Test 253-11	Test 562-15

Tests with high temperature and high pressure capsules (stagnant)

Test 1111-2	Test 1111-9-2	Test 1202	Test 1211
Test 1111-3	Test 1111-9-3	Test 1203	Test 1212
Test 1111-5	Test 1111-9-4	Test 1204	Test 1213
Test 1111-6	Test 1111-9-5	Test 1209	Test 1214
Test 1111-7	Test 1201	Test 1210	Test 1217

Tests with high temperature and high pressure capsules (loop)

Test 2111-6-1	Test 2211-2-2	Test 2211-5	Test 2411-1
Test 2111-6-2	Test 2211-2-3	Test 2311-1	Test 2411-2
Test 2111-6-3	Test 2211-2-4	Test 2311-2	Test 2411-3
Test 2211-1-1	Test 2211-3-1	Test 2311-3	
Test 2211-1-2	Test 2211-3-2	Test 2311-4	
Test 2211-2-1	Test 2211-4	Test 2311-5	

Irradiated fuel tests:

JMTR pre-irradiated fuel tests:

Test JM-1	Test JM-7	Test JM-13	Test JMH-2
Test JM-2	Test JM-8	Test JM-14	Test JMH-3
Test JM-3	Test JM-9	Test JM-15	Test JMH-4
Test JM-4	Test JM-10	Test JM-16	Test JMH-5
Test JM-5	Test JM-11	Test JMN-1	
Test JM-6	Test JM-12	Test JMH-1	

3. Analysis of Experimental Results

3.1 Characteristic Parameters for Cladding Temperature Behavior

In this section, three kinds of characteristic parameters were extracted from the temperature data measured by the cladding surface TCs for summarizing the effects of cooling conditions and cladding pre-irradiation on film-boiling heat transfer from the cladding surface: cladding peak temperature, film boiling time, and cladding-surface superheat at quench. The peak temperature is defined as the maximum value of cladding surface temperature T_c in the transient record. The film boiling time is defined as the duration that $T_c > T_{sat} + 300$ K, where T_{sat} is the saturation temperature of coolant water at a given coolant pressure. The surface superheat at quench is defined as $T_c - T_{sat}$ at the onset of the discontinuous drop in T_c observed at the end of film boiling.

It should be noted that T_c in the foregoing definitions is not from the direct temperature reading of cladding surface TCs. The TC reading of cladding surface temperature does not show the actual cladding temperature. In the case of film boiling duration, the TC temperature is lower than the actual cladding surface temperature. This underestimation is due to the fin-cooling effect of the TCs: temperature drop caused by the TC wires attached to cladding surface [7]. Hence, T_c was determined by $T_c = T_{TC} - \Delta T$, where T_{TC} is the direct temperature reading and ΔT is the temperature drop by the fin effect. The value of ΔT was estimated in conformity with the Tsuruta's model, which had been validated against cladding temperatures determined by metallographic examination of the cladding and ZrO_2 layer thickness [8]. The temperature drop ΔT was estimated to range from ~0 to 250 K, depending on the cladding surface temperature, coolant subcooling, coolant pressure, and diameter of the TC wire.

3.2 Evaluation of Fuel Enthalpy

The characteristic parameters defined in the previous section were plotted against the peak fuel enthalpies in Figs 3.1-52. The peak fuel enthalpy was evaluated based on the total amount of fissile materials (U-235, Pu-239 and Pu-241) in the test fuel rod as follows. First, a coupling factor, corresponding to fission number density in the test fuel per unit integrated NSRR power, was evaluated from neutron transport calculations with the TWODANT code, [9] which considers the configurations of the NSRR core, test capsule, coolant, test fuel rod and so on. Second, the fuel energy deposition was calculated by multiplying this coupling factor to the integrated NSRR power during the pulse-irradiation. Finally, the peak fuel enthalpy, which corresponds to the maximum increase of fuel enthalpy brought by the pulse-irradiation, was evaluated from the fuel energy deposition using an empirical correlation obtained from the NSRR experiments. [10]

In the case of the pre-irradiated-fuel test rod, the total amount of fissile materials

was evaluated from mass analyses on the test fuel. Elemental and isotopic compositions of the test fuel are evaluated from burnup calculations with the SWAT code [11]. The neutron spectrum used in the burnup calculations were adjusted so that the results of mass analyses would be reproduced by the SWAT calculation. The fuel composition obtained in the final calculation was used for the forementioned TWODANT calculation. The results will be summarized and published.

In the case of the tests with high coolant pressure and forced flow condition, the TWODANT calculation was not employed for evaluating the coupling factor, since the calculation model for the high pressure loop system had not been validated. Instead, the coupling factor was determined so that the calculated fuel energy deposition agreed with the experimental value which was evaluated by the procedure based on the short-life fission-product measurement [12].

3.3 Treatment of Iterative Pulse-irradiation Experiment Results

The results of iterative pulse-irradiation experiments were treated separately in Figs.3.1-52, since significant difference in cladding surface temperature had been observed in some cases between the 1st pulse-irradiation and the latter pulse irradiations when a series of pulse-irradiations had been conducted on an identical test fuel rod. In the figures, a legend with an asterisk like “Fresh*” denotes the result of the 2nd, 3rd, or the latter pulse irradiation in an iterative pulse-irradiation experiment. A legend “Fresh” without an asterisk denotes the result of a non-iterative pulse-irradiation experiment or the result of the 1st pulse-irradiation in an iterative pulse-irradiation experiment. A legend “Irrad.” denotes the result of a pulse-irradiation experiment on a fuel rod irradiated in the JMTR.

3.4 Effect of Coolant Subcooling

Figs.3.1-6 compare the cladding peak temperatures between the test groups with fresh fuel, different coolant subcoolings, and similar coolant pressures and flow velocities. It can be seen that the peak temperature decreases with increasing coolant subcooling. The degree of temperature decrease seems not significantly influenced by coolant pressure or flow velocity.

Figs.3.7-12 compare the film boiling times between the test groups with fresh fuel, different coolant subcoolings, and similar coolant pressures and flow velocities. The effect of coolant subcooling is more clearly seen in the film boiling time than in the peak temperature; the film boiling time significantly decreases with increasing coolant subcooling. The degree of film-boiling-time decrease is larger at atmospheric pressure coolant condition than at high pressure conditions, while it seems not influenced by coolant flow velocity.

Figs.3.13-17 compare the surface superheats at quench between the test groups

with fresh fuel, different coolant subcoolings, and similar coolant pressures and flow velocities. It can be seen that the surface superheat at quench increases with coolant subcooling except the test groups with high coolant pressure and forced flow conditions (see Fig.3.17).

The surface superheat at quench tends to increase with also peak fuel enthalpy in the test group with stagnant coolant, atmospheric coolant pressure, and coolant subcooling of ~80 K (see Fig.3.13). Such a dependency on peak fuel enthalpy could be attributed to some changes in cladding surface conditions due to high-temperature oxidation during film boiling. For example, the effect of surface-wettability increase on the quench behavior was pointed by Sugiyama et al.[13] On the other hand, the surface superheat at quench seems not dependent on peak fuel enthalpy in the test group with stagnant coolant, atmospheric coolant pressure, and coolant subcooling of ~10 K (see Fig.3.13) and in the test group with flow velocity of ~1.8 m/s, atmospheric coolant pressure, and coolant subcoolings of ~80K (see Fig.3.15).

3.5 Effect of Coolant Pressure

Figs.3.18-23 compares the cladding peak temperatures between the test groups with fresh fuel, different coolant pressures, and similar coolant subcoolings and flow velocities. It can be seen that the peak temperature decreases with increasing coolant pressure except the test groups with stagnant coolant and coolant subcoolings more than ~20 K (see Figs.3.19 and 20). The coolant subcoolings of the test groups compared in Fig.3-23 are different each other to some degree, but the separate effect of coolant pressure on the peak temperatures can be clearly seen in the figure; the test group with atmospheric pressure gives higher peak temperature than the other test groups with coolant pressures of ~7 MPa and ~16 MPa irrespective of its high subcooling (~80 K). On the whole, the effect of coolant pressure seems to become more important at lower pressure or higher coolant flow conditions.

Figs.3.24-29 compare the film boiling times between the test groups with fresh fuel, different coolant pressures, and similar coolant subcoolings and flow velocities. The effect of coolant pressure is seen in the test groups with stagnant coolant and coolant subcooling of ~10 K, coolant flow velocity of ~0.6–0.7 m/s and coolant subcoolings of ~20 K, and coolant flow velocity of ~1.0 m/s and coolant subcoolings of ~20 K (see Figs.3.24, 27, and 28); the film boiling time significantly decreases with increasing coolant pressure. The film boiling time seems not dependent on coolant pressure in the other test groups as shown in Fig.3.25, 26, and 29. These results suggest that the effect of coolant pressure is suppressed under high coolant subcooling conditions, while it seems not influenced by coolant flow velocity.

Figs.3.30-35 compare the surface superheats at quench between the test groups with fresh fuel, different coolant pressures, and similar coolant subcoolings and flow

velocities. The surface superheat decreases with increasing coolant pressure in all the test groups with forced flow conditions, and in the test group with stagnant coolant and coolant subcooling of ~20-30 K (see Figs 3.31, 33-35). The pressure effect is not clear in the test groups with stagnant coolant and coolant subcoolings of ~10 K and ~80 K (see Figs 3.30 and 32).

3.6 Effect of Coolant Flow Velocity

Figs.3.36-40 compare the cladding peak temperatures between the test groups with fresh fuel, different coolant flow velocities, and similar coolant subcoolings and pressures. The effect of coolant flow velocity is not clearly seen in the test groups with coolant subcoolings of ~10 K regardless of coolant pressure (see Fig.3.36-38). In the case of the test groups with high coolant pressure and coolant subcoolings more than ~20 K, the effect of coolant flow velocity can be seen (see Figs.3.39 and 40); the peak temperature decreases with increasing coolant flow velocity.

Figs.3.41-45 compare the film boiling times between the test groups with fresh fuel, different coolant flow velocities, and similar coolant subcoolings and pressures. The film boiling time decreases with increasing coolant flow velocity in the test groups with atmospheric coolant pressure and coolant subcooling of ~80 K (see Fig.3.42). The effect of coolant flow velocity is not clear in the rest cases for which film boiling times are compared.

Figs.3.46-49 compare the surface superheats at quench between the test groups with fresh fuel, different coolant flow velocities, and similar coolant subcoolings and pressures. At atmospheric pressure, the surface superheat at quench seems to decrease with increasing coolant flow velocity under the low coolant subcooling of ~20 K (see Fig.3.46), while the effect of coolant flow velocity is not clearly seen under the high coolant subcooling of ~80 K (see Fig.3.47). At high pressure of ~7 MPa, the surface superheat at quench seems to decrease with increasing coolant flow velocity under the coolant subcooling of ~20–30 K (see Fig.3.49), while the effect of coolant flow velocity is not clearly seen under the coolant subcooling of ~10 K (see Fig.3.48).

3.7 Effect of Cladding Pre-irradiation

Fig.3.50 compares the cladding peak temperatures between the fresh fuel and the pre-irradiated fuel test groups with similar cooling conditions. A remarkable effect of pre-irradiation is seen in the test group with atmospheric coolant pressure, stagnant coolant, and coolant subcooling of ~80 K (see Fig.3.50); the peak temperatures in the pre-irradiated fuel tests are significantly lower than those in the fresh fuel tests.

Fig.3.51 compares the film boiling times between the fresh fuel and the pre-irradiated fuel test groups with similar coolant conditions. The film boiling times in the pre-irradiated fuel tests are much shorter than those in the fresh fuel tests in the case of

the test groups with atmospheric coolant pressure and coolant subcooling of ~80 K (see Fig.3.51).

Fig.3.52 compares the surface superheats at quench between the fresh fuel and the pre-irradiated fuel test groups with similar cooling conditions. The effect of pre-irradiation on surface superheat at quench is not clearly seen.

4. Summary

The NSRR-experiment results have indicated that the heat transfer from the fuel rod surface to the coolant water is enhanced, on the whole, with increasing the coolant subcooling, the coolant pressure, and the coolant flow velocity, and with the pre-irradiation of the fuel rod. The coolant subcooling is an effective parameter on the heat transfer regardless of the other cooling conditions: coolant pressure and the flow velocity. The effectiveness of the coolant pressure seems dependent on the other coolant conditions, and so does the coolant flow velocity. The effect of pre-irradiation is remarkable, though the corresponding experiments cover the coolant condition with atmospheric pressure, stagnant water, and subcooling of ~80 K alone. The present NSRR-experiment data will be used for the validation of the new heat transfer model for the RANNS code, which is now under development.

Acknowledgements

This work is based on the huge database of the NSRR experiments, which has been extended since the first test was performed in 1975. Authors would like to acknowledge and express their appreciation for the effort devoted by all the engineers, technicians and researchers involved in the NSRR program.

References

1) N.Ohnishi, K.Ishijima and S.Tanzawa : “A study of subcooled film-boiling heat transfer under reactivity-initiated accident conditions in light water reactor”, Nucl. Sci. Eng., 88, pp.331-341 (1984).
2) S.Saito et al. : “Measurement and Evaluation on Pulsing Characteristics and Experimental Capability of NSRR”, J. Nucl. Sci. Technol. 14, 3, pp.226-238 (1977).
3) M.Ishikawa and S. Shiozawa : “A Study of Fuel Behavior under Reactivity Initiated Accident Conditions – Review”, J. Nucl. Mater., 95, pp.1-30 (1980).
4) S. Kobayashi and S. Toyokawa : “NSRR High-Temperature and High-Pressure Capsule”, JAERI-M 8767 (1980).
5) S. Tanzawa, T. Kikuchi and T. Fujishiro : “Fabrication and Performance Tests of NSRR High-Temperature and High-Pressure Loop”, JAERI-M 83-039 (1983).
6) K.Ishijima et al. : “Experimental Data Report for Test JM-1”, JAERI-M 91-127 (1991).
7) T.Tsuruta et al. : “Evalulation of Thermocouple Fin Effect in Cladding Surface Temperature Measurement during Film Boiling”, J. Nucl. Sci. Technol., 21, pp.515-527 (1984).

8) S.Shiozawa et al. : "Zircaloy-UO_2 and -Water Reactions and Cladding Temperature Estimation for Rapidly-Heated Fuel Rods under an RIA Condition", J. Nucl. Sci. Technol., 19, pp.368-383 (1982).
9) R.E.Alcouffe et al. : "User's Guide for TWODANT: A Code Package for Two-Dimensional, Diffusion Accelerated, Neutral Particle Transport", LA-10049-M, Revised, (1990).
10) T.Fuketa et al. : "Analysis of Energy Deposition and Evaluation of Maximum Load of Irradiation Capsule for NSRR Experiment with Uranium-Zirconium Hydride Fuel", JAERI-Research 95-005 (1995).
11) K.Suyama et al. : "Revised SWAT ― The Integrated Burnup Calculation Code System ―", JAERI-Data/Code 2000-027 (2000).
12) T.Nakamura et al. : "Evaluation of Energy Depositions in the NSRR Irradiated Fuel Tests (Tests with Fuel Rods Pre-irradiated in the JMTR)", JAERI-Research 98-052 (1998).
13) T.Sugiyama et al. : "Effect of Cladding Surface Pre-oxidation on Rod Coolability under Reactivity Initiated Accident Conditions", J. Nucl. Sci. Technol., 41, pp.1083-1090 (2004).

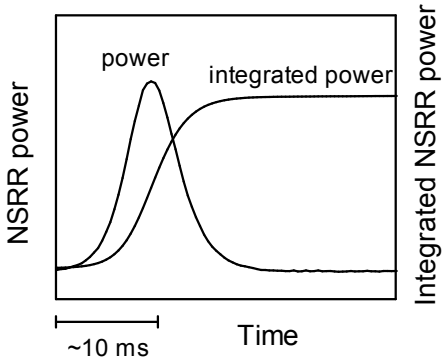

Fig.2.1 Typical histories of NSRR power and time-integrated NSRR power in RIA test

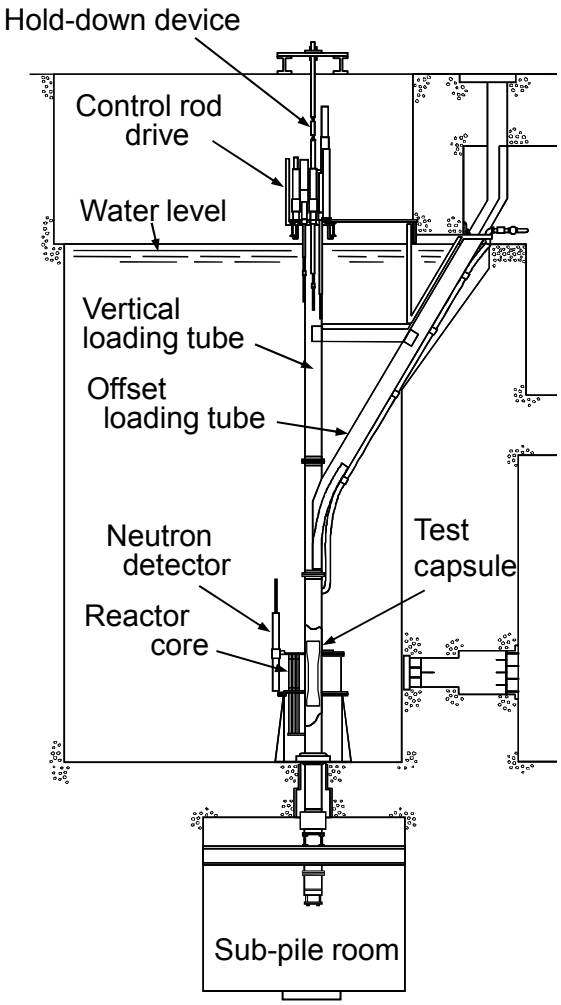

(a) Vertical cross section of NSRR

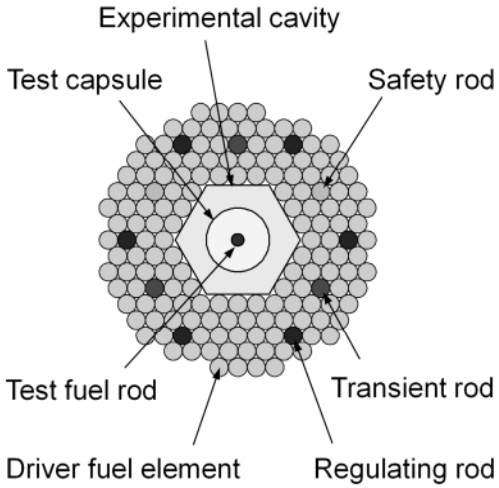

(b) Horizontal cross section of NSRR core

Fig.2.2 Outline of NSRR

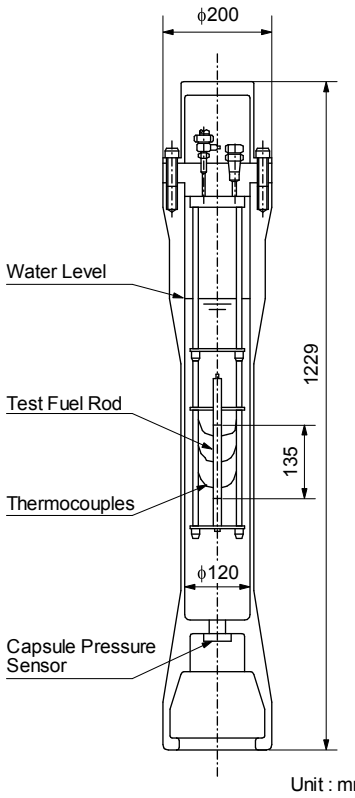

Fig.2.3 Capsule for fresh fuel test at room temperature and atmospheric pressure

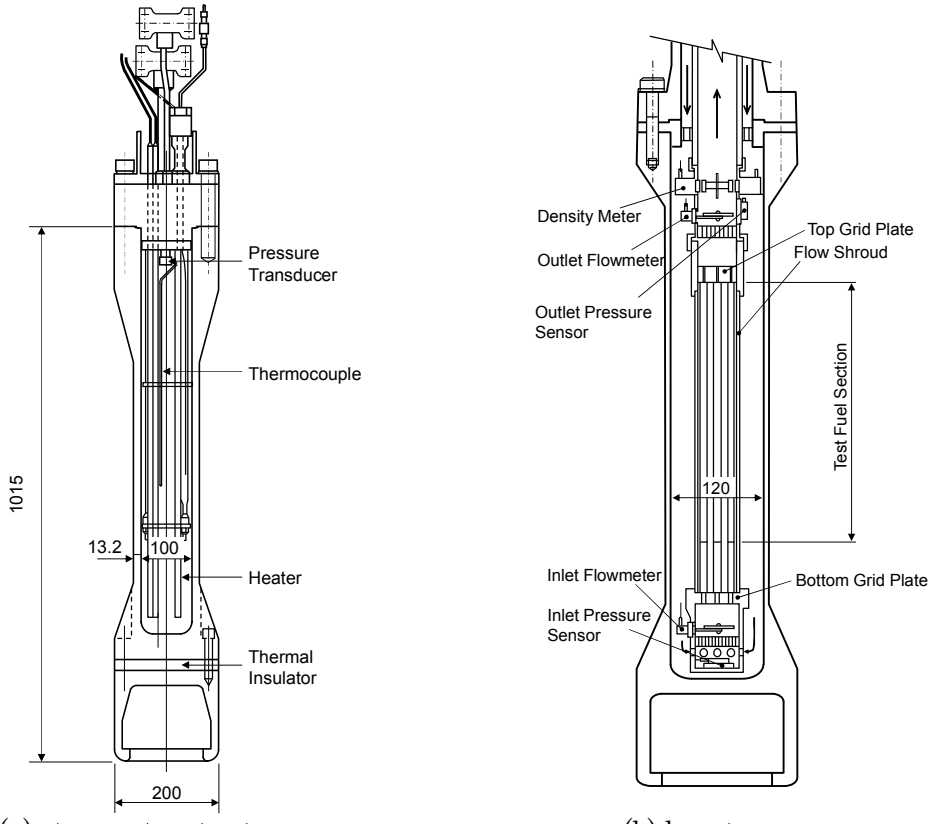

(a) stagnant water type (b) loop type

Fig.2.4 Capsules for fresh fuel test at high temperature and high pressure

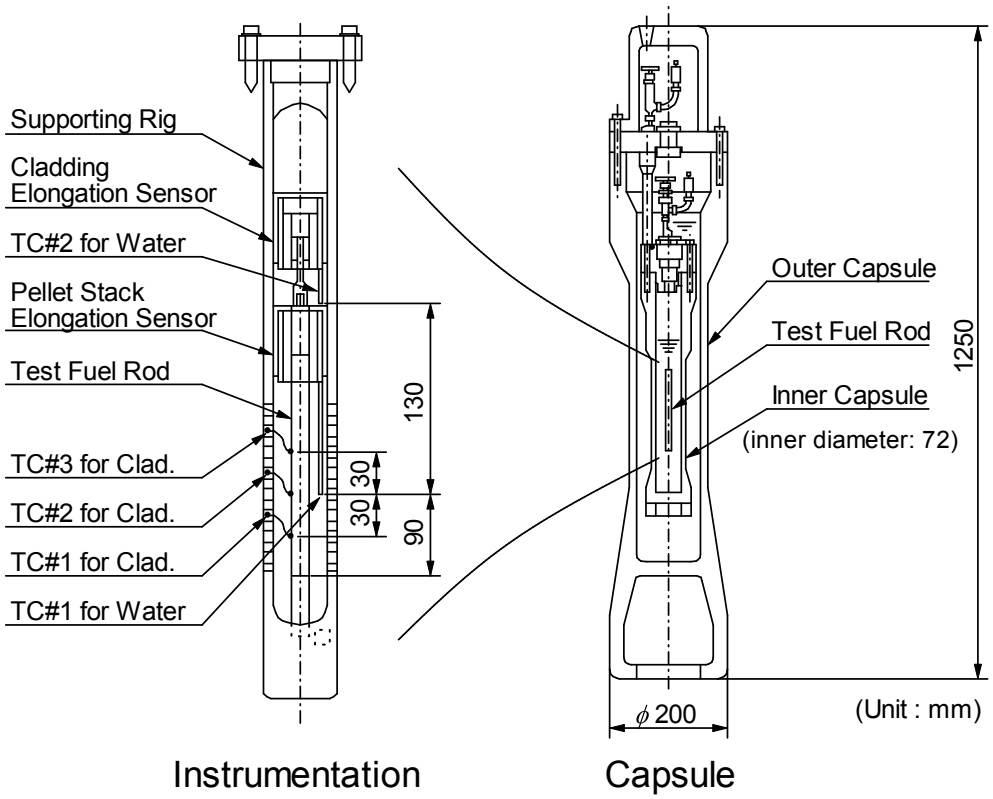

Fig.2.5　Capsules for JMTR pre-irradiated fuel test

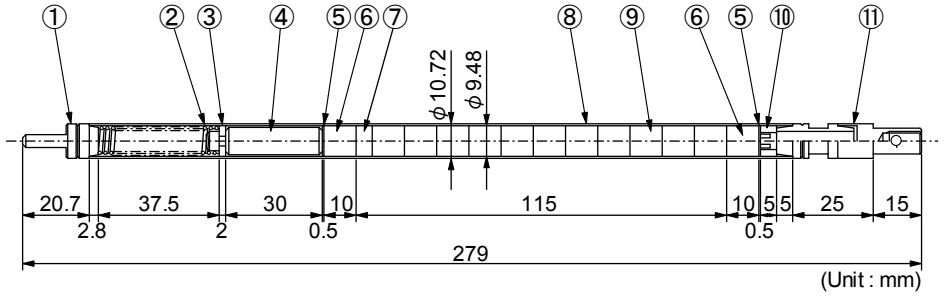

6	Fuel Pellet	UO_2	Natural				
5	Disk	SUS304		11	Bottom End Fitting	Zry-4	
4	Iron Core	Magnetic Iron		10	Spacer	SUS304	
3	Spring Adaptor	SUS304		9	Fuel Pellet	UO_2	10%E
2	Spring	Inconel-X		8	Cladding Tube	Zry-4	
1	Top End Fitting	Zry-4		7	Half Pellet	UO_2	10%E
ITEM	DESCRIPTION	MATERIAL	NOTE	ITEM	DESCRIPTION	MATERIAL	NOTE

Fig.2.6 Design of NSRR standard test fuel rod for fresh fuel test
Cladding outer / inner diameter: 10.72 / 9.48 (mm)
Pellet diameter / height: 9.29 / 10.0 (mm)

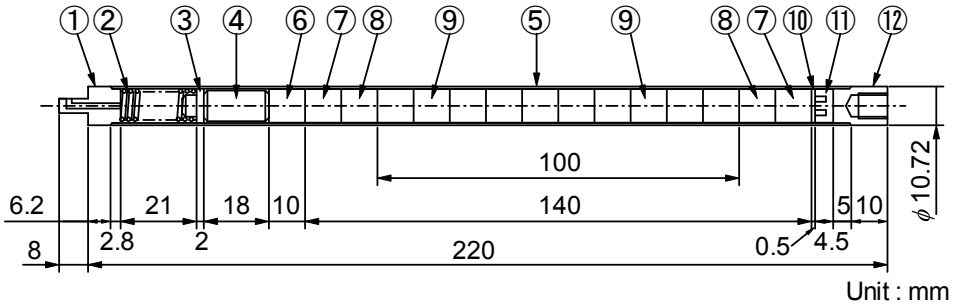

6	Alumina pellet	Al_2O_3	1	12	Bottom end fitting	Zry-4	1
5	Cladding tube	Zry-4	1	11	Spacer	SUS304	1
4	Magnetic iron core	MEIF	1	10	Disk	SUS304	1
3	Spring holder	SUS304	1	9	UO_2 pellet	UO_2(10%E*)	10
2	Spring	Inconel	1	8	UO_2 pellet	UO_2 (5%E)	2
1	Top end fitting	Zry-4	1	7	UO_2 pellet	UO_2(Natural)	2
No.	Item	Material	Parts	No.	Item	Material	Parts

* 20%E for JMH tests

Fig.2.7 Design of JMTR pre-irradiated fuel rod
Cladding outer / inner diameter: 10.72 / 9.48 (mm)
Pellet diameter / height: 9.29 / 10.0 (mm)

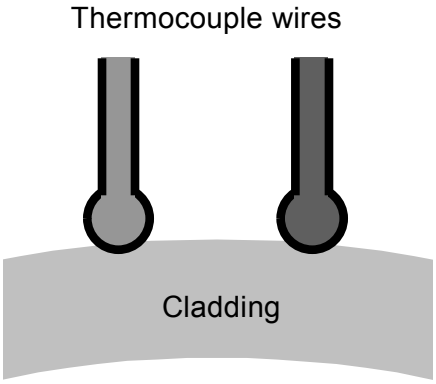

(a) Welding of cladding surface thermocouple (horizontal cross-section)

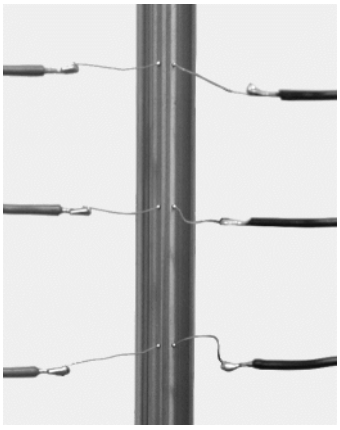

(b) Appearance of cladding surface thermocouples

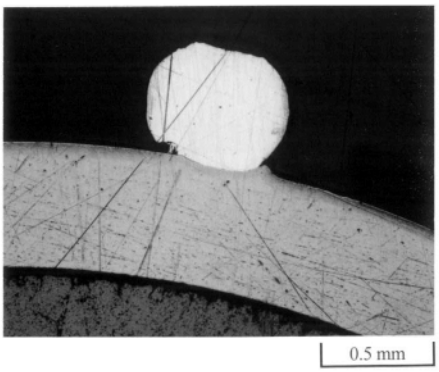

(c) Cladding cross-section at the thermocouple welding elevation
(#4 TC in Test 562-10, after pulse-irradiation)

Fig.2.8　Thermocouple attachment on the cladding surface

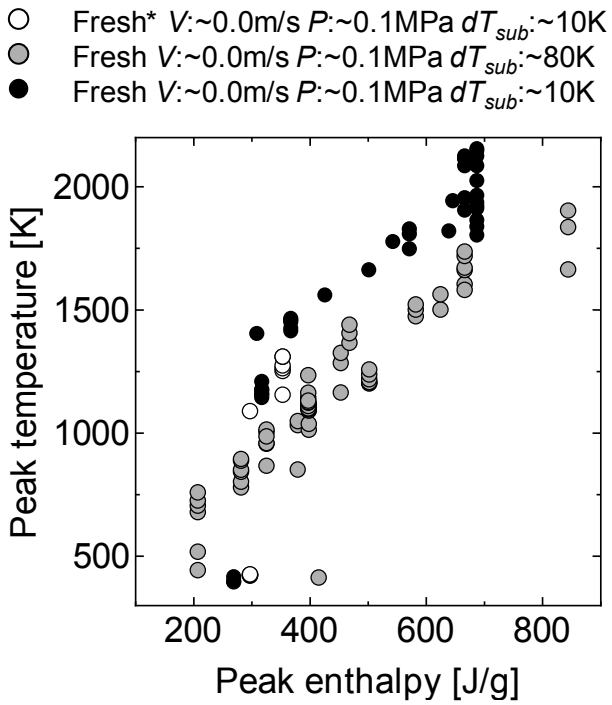

Fig.3.1 Peak temperatures for test cases with fresh fuel, stagnant coolant, atmospheric coolant pressure, and coolant subcoolings of ~10–80 K (* : iterative pulse-irradiation experiment)

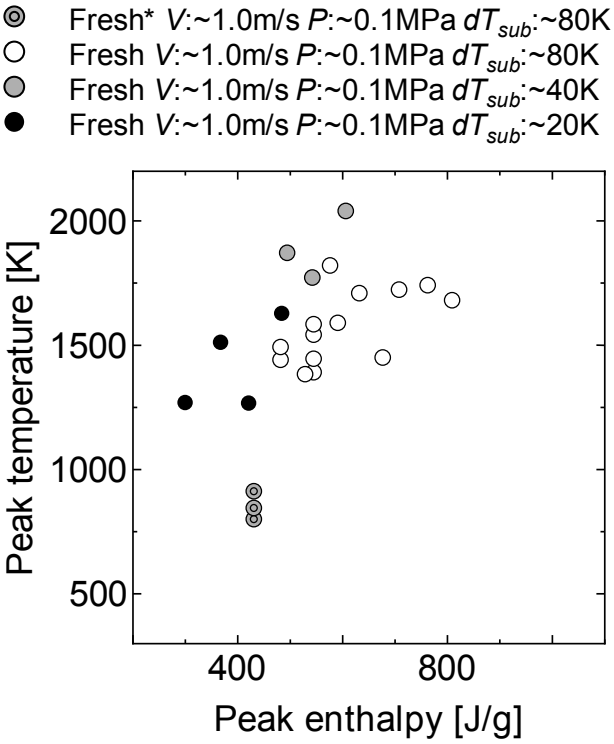

Fig.3.2 Peak temperatures for test cases with fresh fuel, coolant flow velocity of ~1.0 m/s, atmospheric coolant pressure, and coolant subcoolings of ~20–80 K (* : iterative pulse-irradiation experiment)

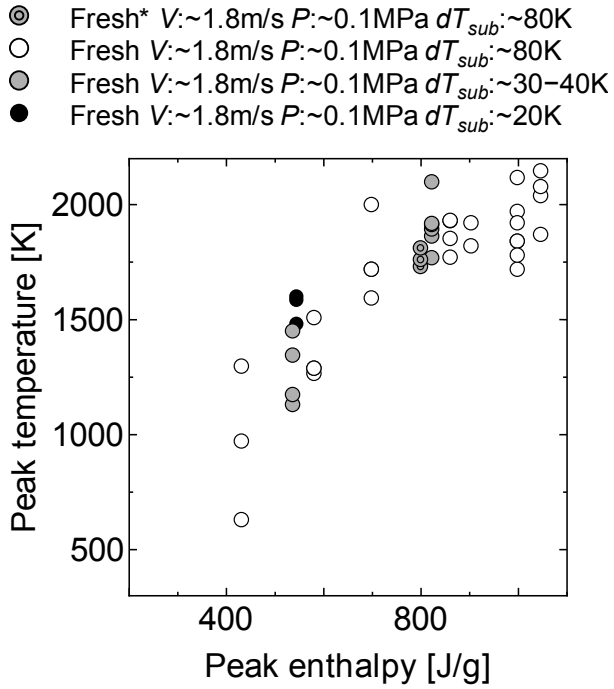

Fig.3.3 Peak temperatures for test cases with fresh fuel, coolant flow velocity of ~1.8 m/s, atmospheric coolant pressure, and coolant subcoolings of ~20–80 K (* : iterative pulse-irradiation experiment)

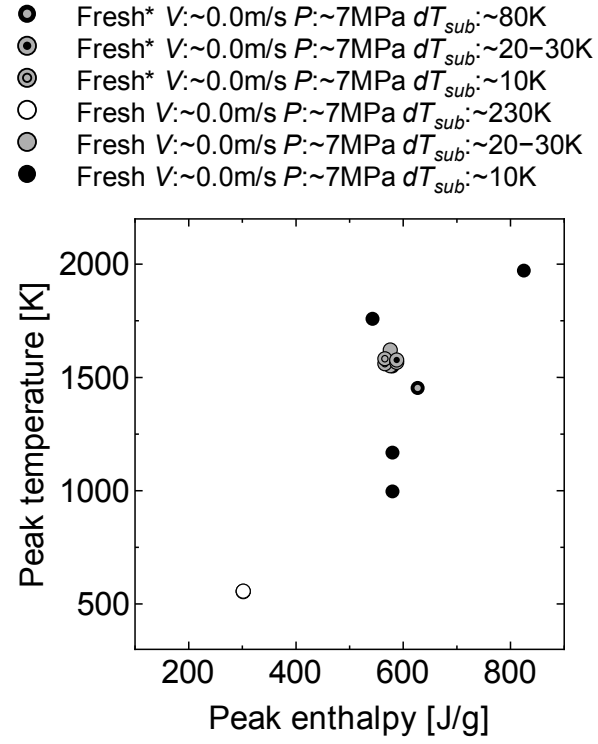

Fig.3.4 Peak temperatures for test cases with fresh fuel, stagnant coolant, coolant pressure of ~7 MPa, and coolant subcoolings of ~10–230 K (* : iterative pulse-irradiation experiment)

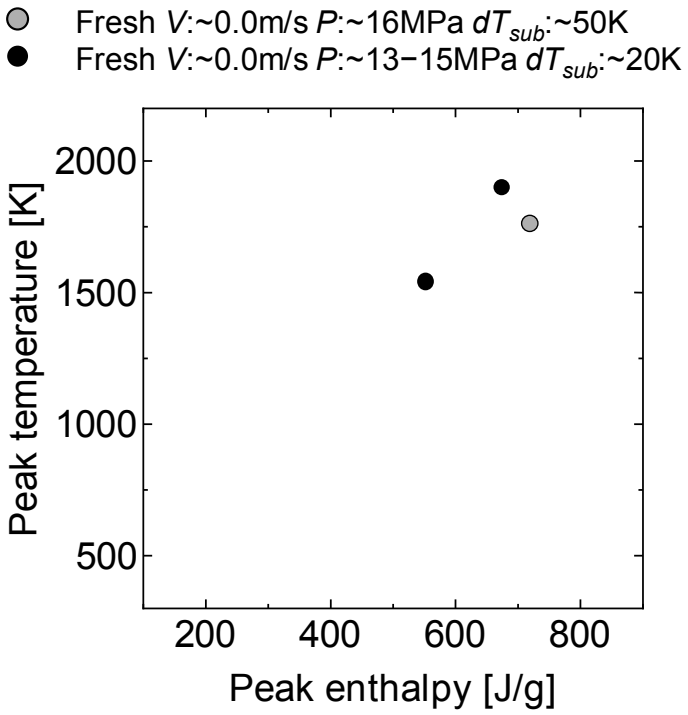

Fig.3.5　Peak temperatures for test cases with fresh fuel, stagnant coolant, coolant pressures of ~13–16 MPa, and coolant subcoolings of ~20–50 K

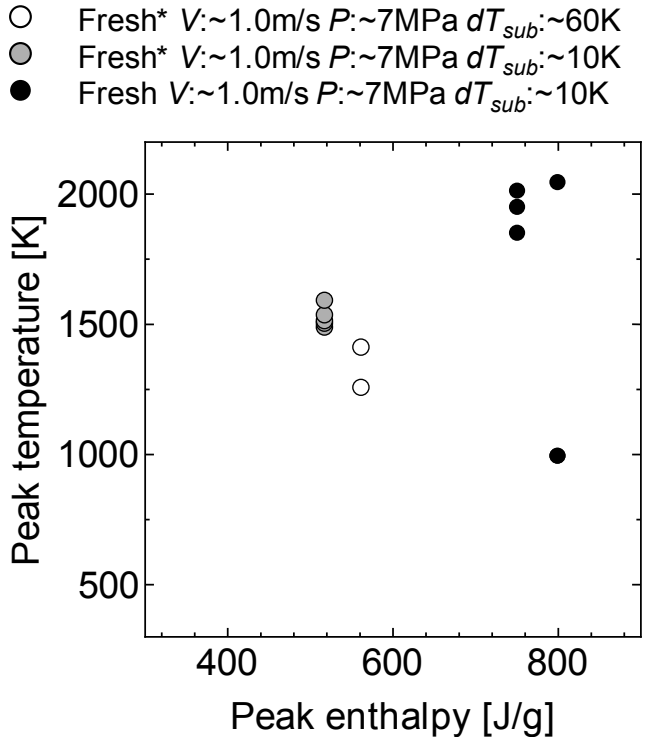

Fig.3.6　Peak temperatures for test cases with fresh fuel, coolant flow velocity of ~1.0 m/s, coolant pressure of ~7 MPa, and coolant subcoolings of ~10–60 K (* : iterative pulse-irradiation experiment)

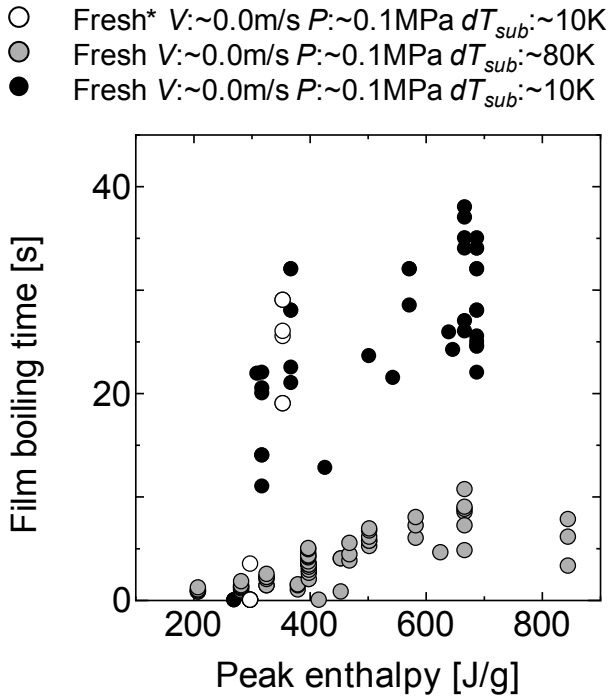

Fig.3.7　Film boiling times for test cases with fresh fuel, stagnant coolant, atmospheric coolant pressure, and coolant subcoolings of ~10–80 K (* : iterative pulse-irradiation experiment)

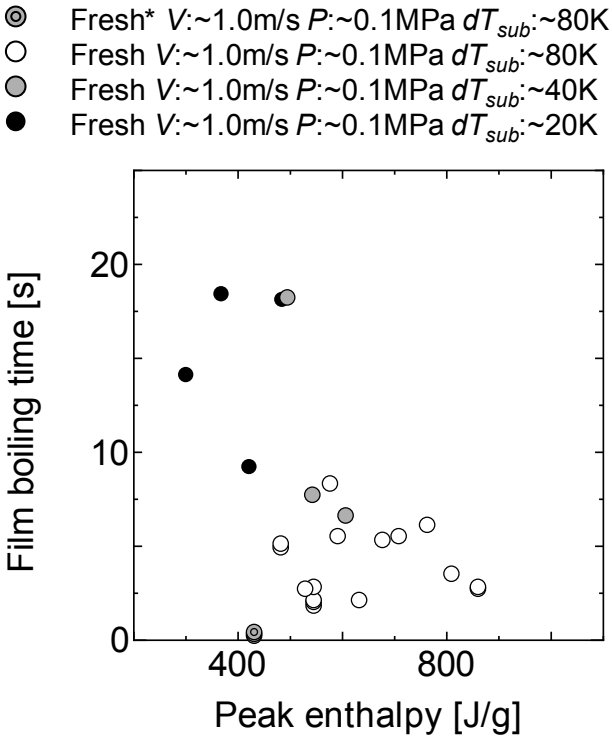

Fig.3.8　Film boiling times for test cases with fresh fuel, coolant flow velocity of ~1.0 m/s, atmospheric coolant pressure, and coolant subcoolings of ~20–80 K (* : iterative pulse-irradiation experiment)

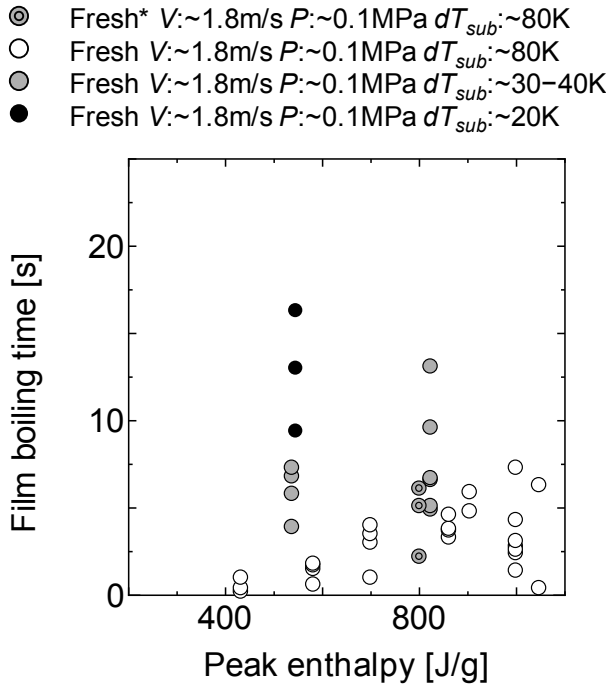

Fig.3.9 Film boiling times for test cases with fresh fuel, coolant flow velocity of ~1.8 m/s, atmospheric coolant pressure, and coolant subcoolings of ~20–80 K (* : iterative pulse-irradiation experiment)

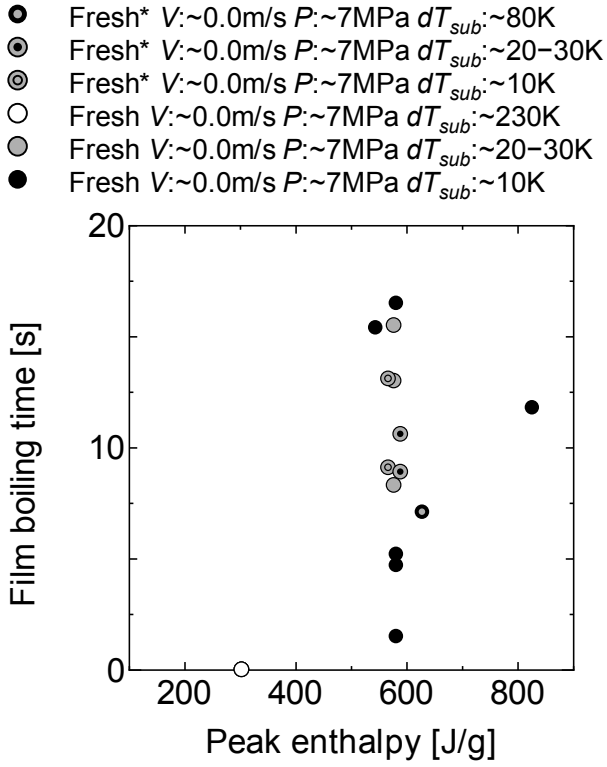

Fig.3.10 Film boiling times for test cases with fresh fuel, stagnant coolant, coolant pressure of ~7 MPa, and coolant subcoolings of ~10–230 K (* : iterative pulse-irradiation experiment)

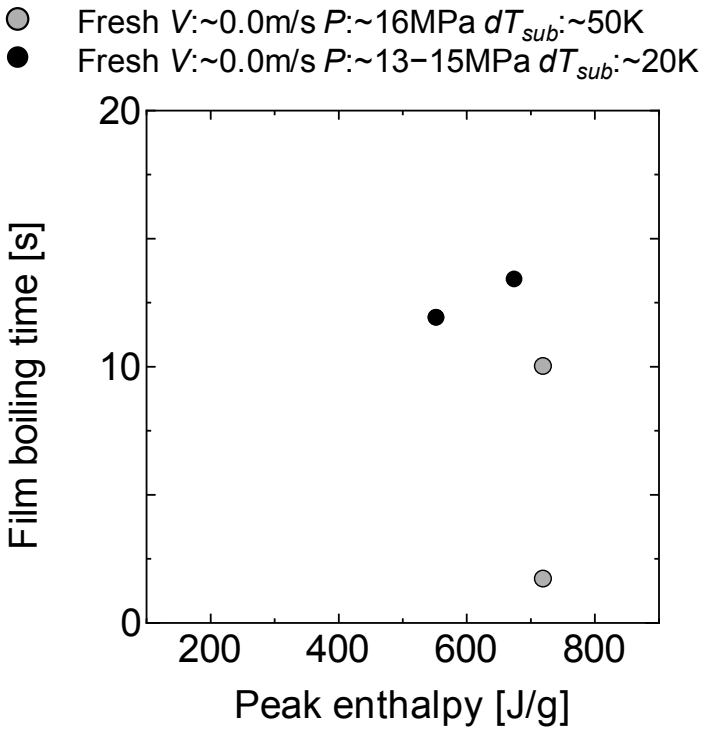

Fig.3.11 Film boiling times for test cases with fresh fuel, stagnant coolant, coolant pressures of ~13–16 MPa, and coolant subcoolings of ~20–50 K

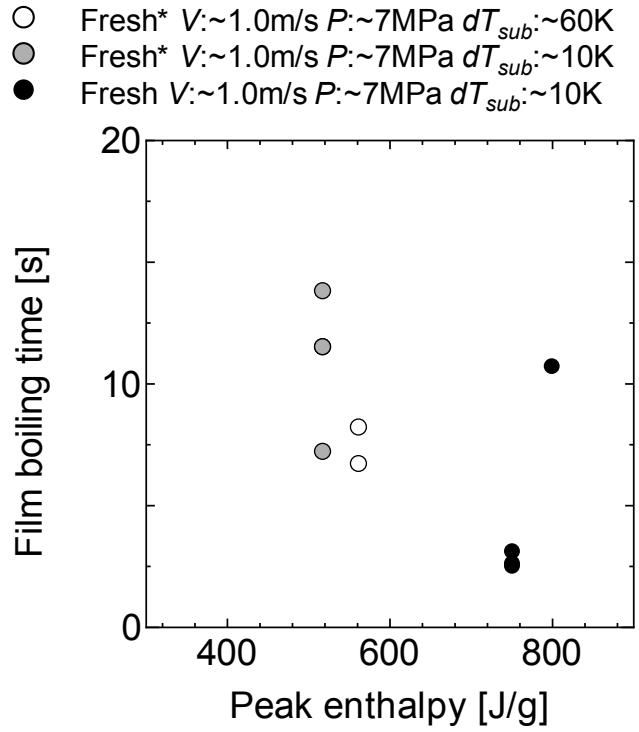

Fig.3.12 Film boiling times for test cases with fresh fuel, coolant flow velocity of ~1.0 m/s, coolant pressure of ~7 MPa, and coolant subcoolings of ~10–60 K (* : iterative pulse-irradiation experiment)

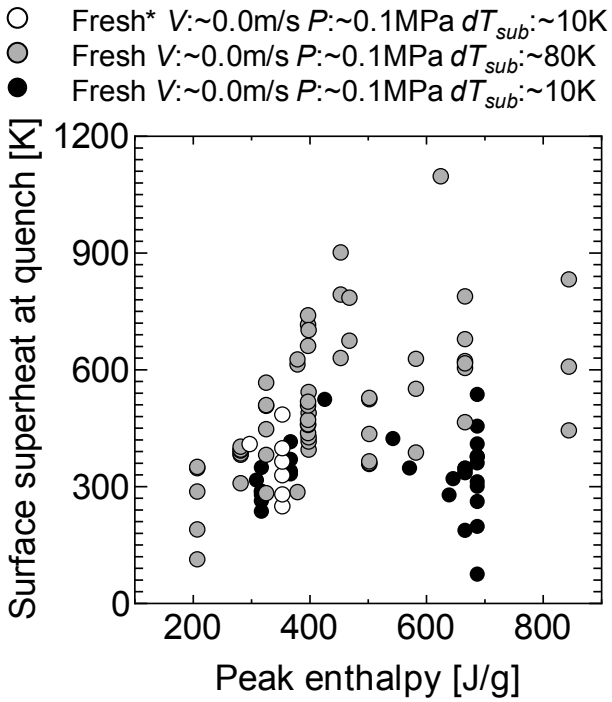

Fig.3.13　Surface superheats at quench for test cases with fresh fuel, stagnant coolant, atmospheric coolant pressure, and coolant subcoolings of ~10–80 K (* : iterative pulse-irradiation experiment)

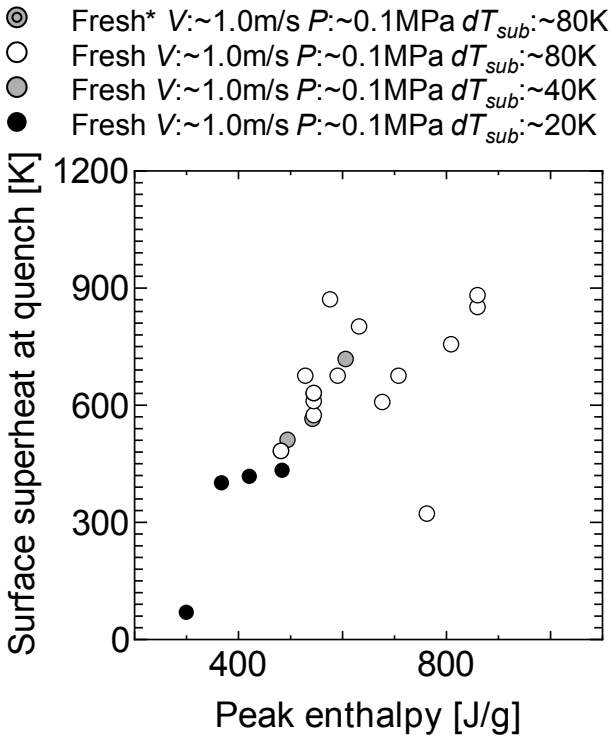

Fig.3.14　Surface superheats at quench for test cases with fresh fuel, coolant flow velocity of ~1.0 m/s, atmospheric coolant pressure, and coolant subcoolings of ~20–80 K (* : iterative pulse-irradiation experiment)

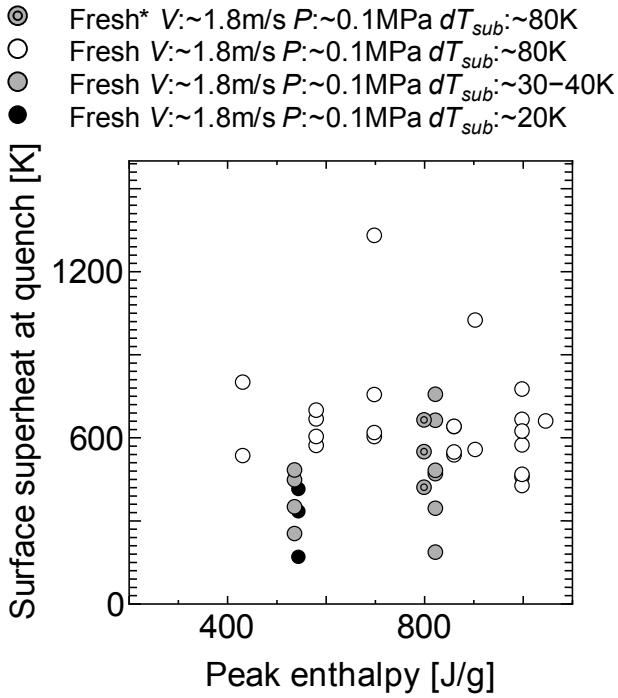

Fig.3.15　Surface superheats at quench for test cases with fresh fuel, coolant flow velocity of ~1.8 m/s, atmospheric coolant pressure, and coolant subcoolings of ~20–80 K (* : iterative pulse-irradiation experiment)

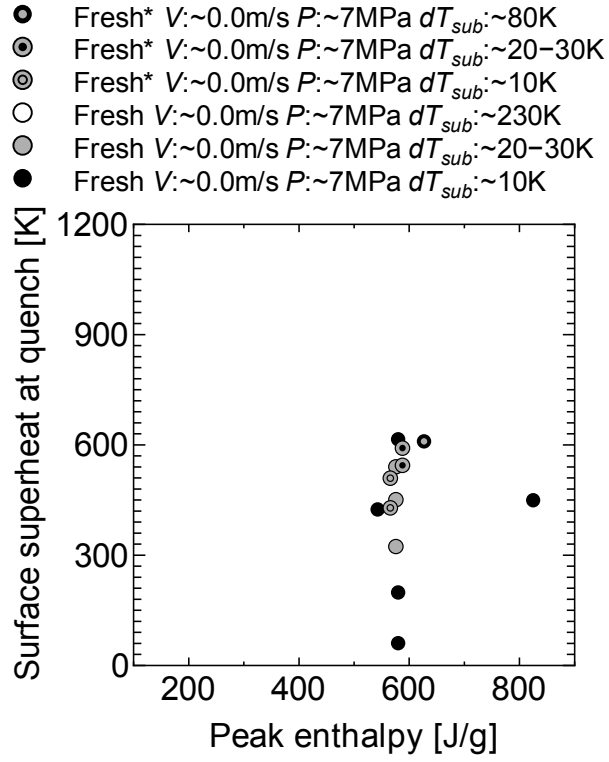

Fig.3.16　Surface superheats at quench for test cases with fresh fuel, stagnant coolant, coolant pressure of ~7 MPa, and coolant subcoolings of ~10–230 K (* : iterative pulse-irradiation experiment)

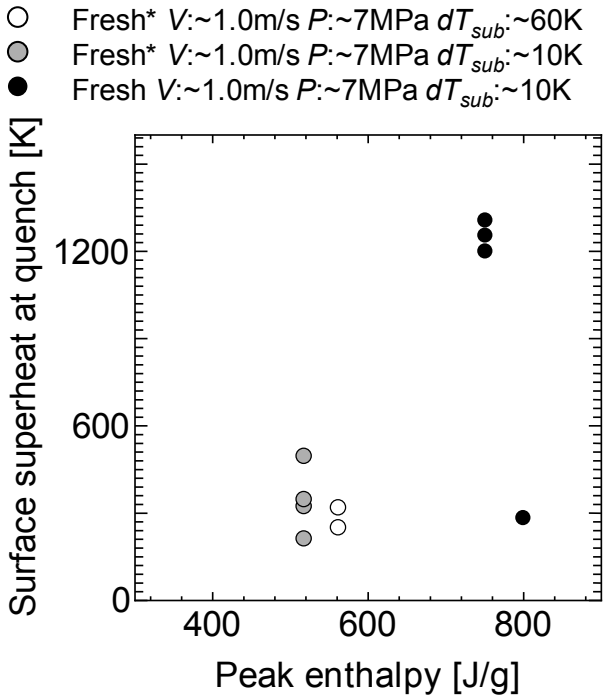

Fig.3.17　Surface superheats at quench for test cases with fresh fuel, coolant flow velocity of ~1.0 m/s, coolant pressure of ~7 MPa, and coolant subcoolings of ~10–60 K (* : iterative pulse-irradiation experiment)

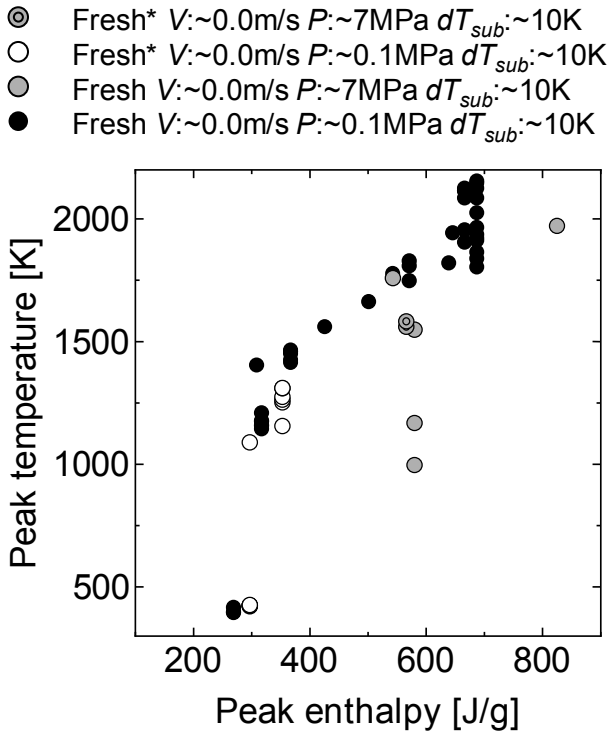

Fig.3.18　Peak temperatures for test cases with fresh fuel, stagnant coolant, coolant pressures of ~0.1–7 MPa, and coolant subcooling of ~10 K (* : iterative pulse-irradiation experiment)

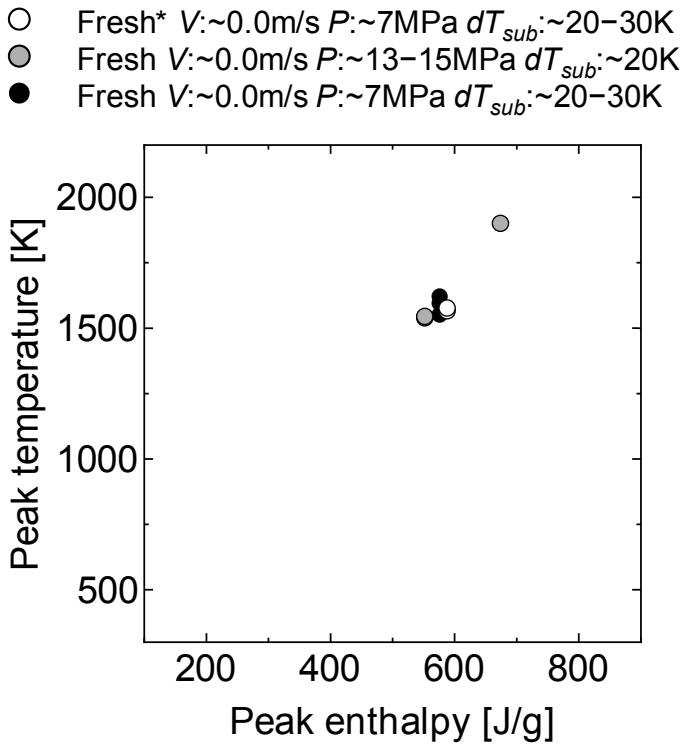

Fig.3.19 Peak temperatures for test cases with fresh fuel, stagnant coolant, coolant pressures of ~7–15 MPa, and coolant subcoolings of ~20–30 K (* : iterative pulse-irradiation experiment)

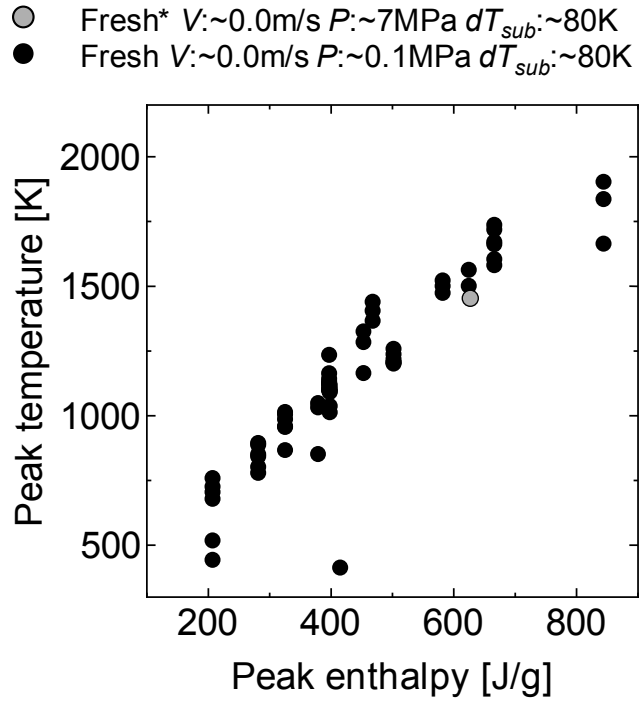

Fig.3.20 Peak temperatures for test cases with fresh fuel, stagnant coolant, coolant pressures of ~0.1–7 MPa, and coolant subcooling of ~80 K (* : iterative pulse-irradiation experiment)

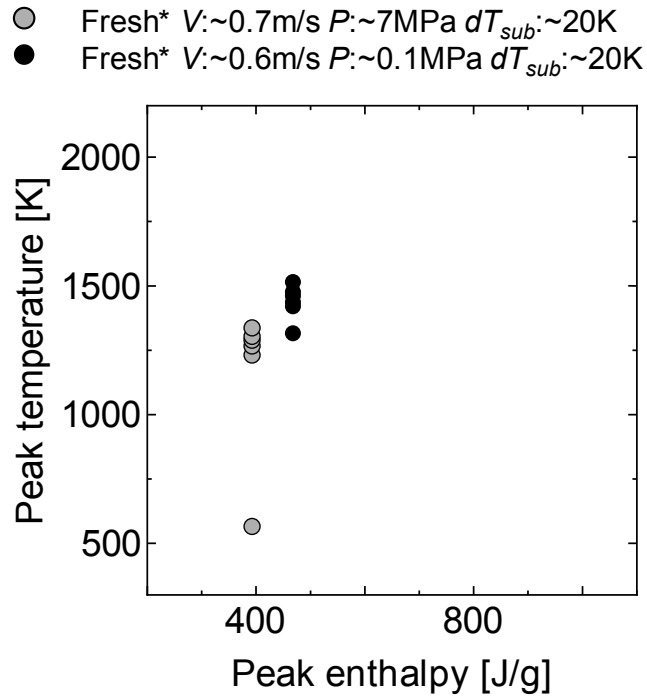

Fig.3.21 Peak temperatures for test cases with fresh fuel, coolant flow velocities of ~0.6–0.7 m/s, coolant pressures of ~0.1–7 MPa, and coolant subcooling of ~20 K (* : iterative pulse-irradiation experiment)

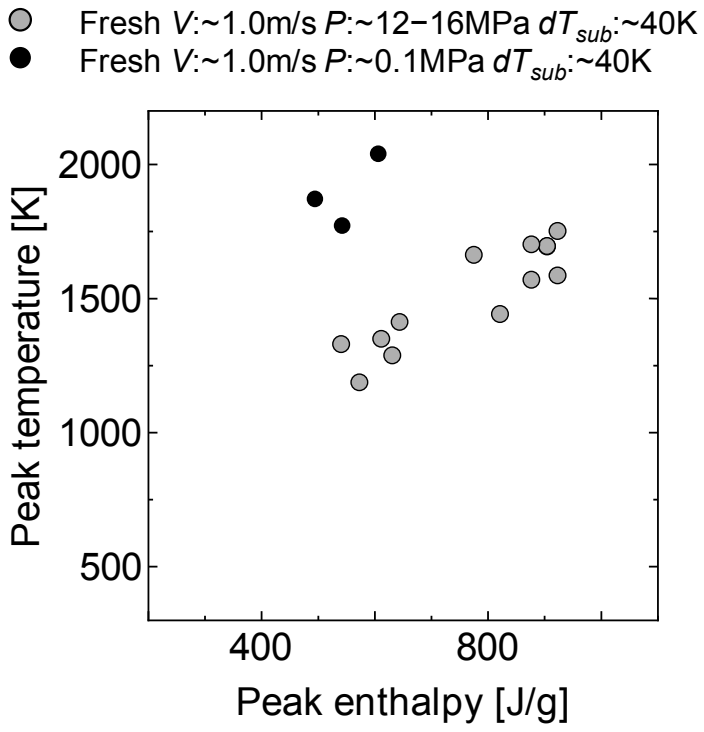

Fig.3.22 Peak temperatures for test cases with fresh fuel, coolant flow velocity of ~1.0 m/s, coolant pressures of ~0.1–16 MPa, and coolant subcooling of ~40 K

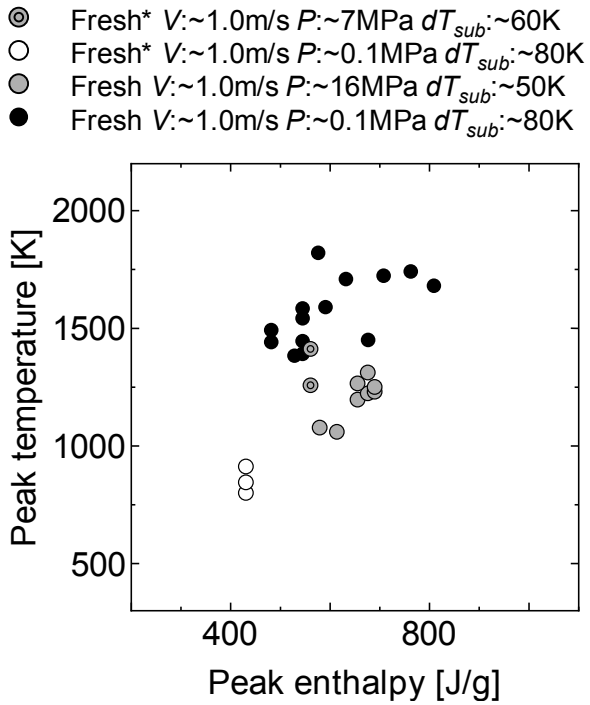

Fig.3.23 Peak temperatures for test cases with fresh fuel, coolant flow velocity of ~1.0 m/s, coolant pressures of ~0.1–16 MPa, and coolant subcoolings of ~50–80 K (* : iterative pulse-irradiation experiment)

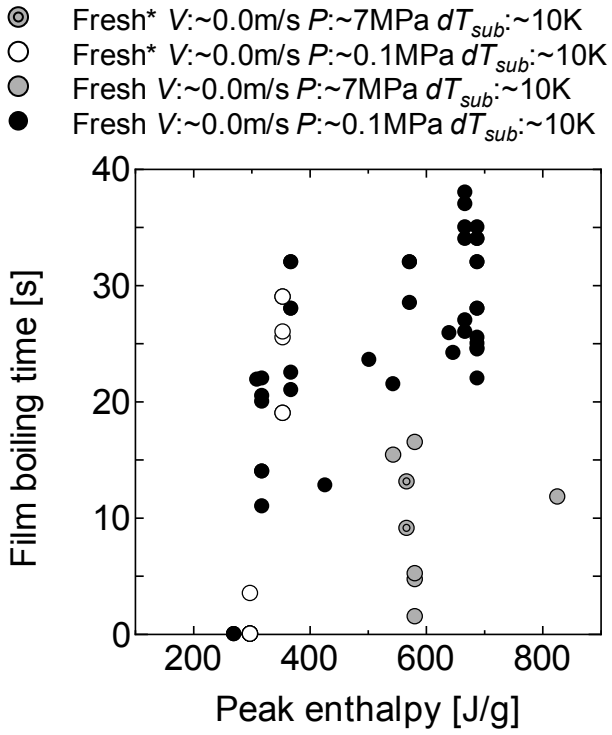

Fig.3.24 Film boiling times for test cases with fresh fuel, stagnant coolant, coolant pressures of ~0.1–7 MPa, and coolant subcoolings of ~10 K (* : iterative pulse-irradiation experiment)

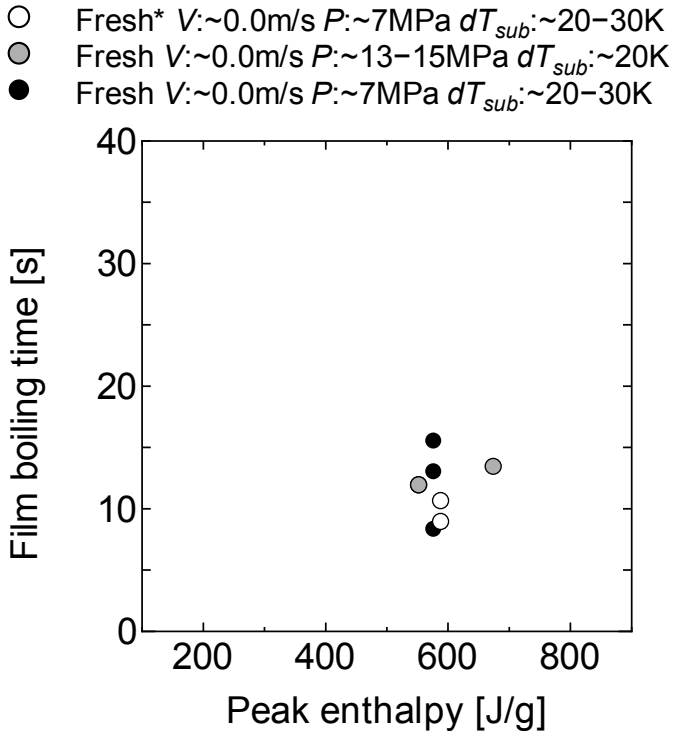

Fig.3.25 Film boiling times for test cases with fresh fuel, stagnant coolant, coolant pressures of ~7–15 MPa, and coolant subcoolings of ~20–30 K (* : iterative pulse-irradiation experiment)

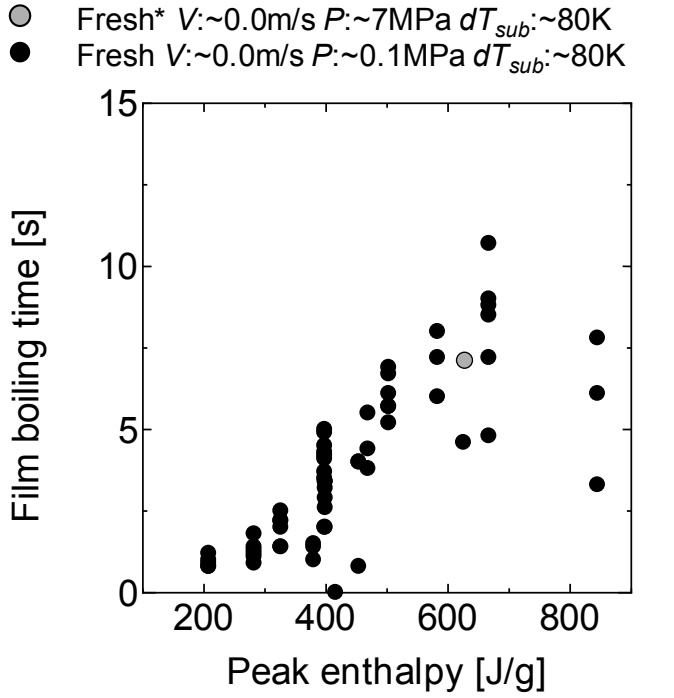

Fig.3.26 Film boiling times for test cases with fresh fuel, stagnant coolant, coolant pressures of ~0.1–7 MPa, and coolant subcooling of ~80 K (* : iterative pulse-irradiation experiment)

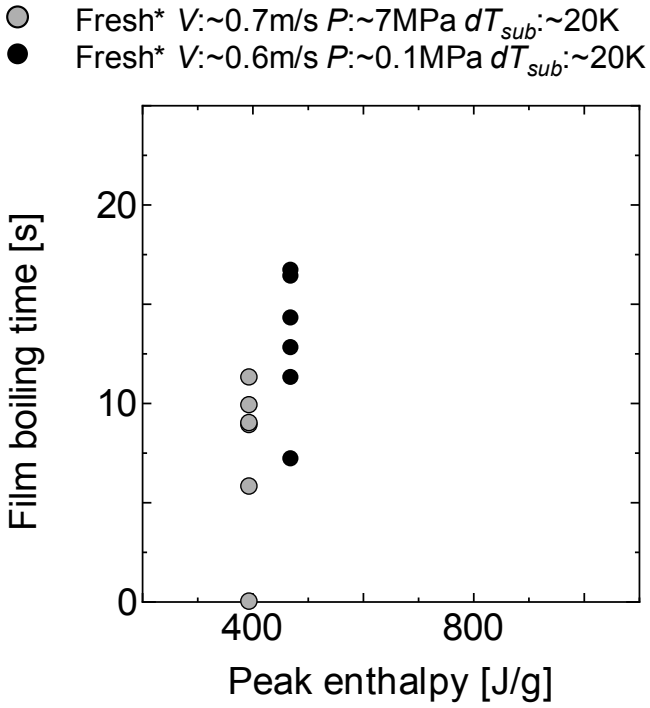

Fig.3.27 Film boiling times for test cases with fresh fuel, coolant flow velocities of ~0.6–0.7 m/s, coolant pressures of ~0.1–7 MPa, and coolant subcooling of ~20 K (* : iterative pulse-irradiation experiment)

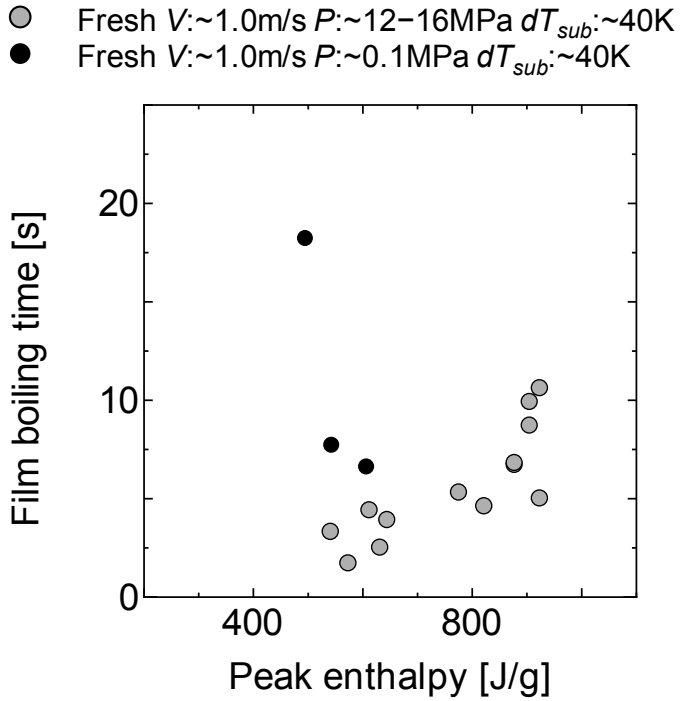

Fig.3.28 Film boiling times for test cases with fresh fuel, coolant flow velocity of ~1.0 m/s, coolant pressures of ~0.1–16 MPa, and coolant subcooling of ~40 K

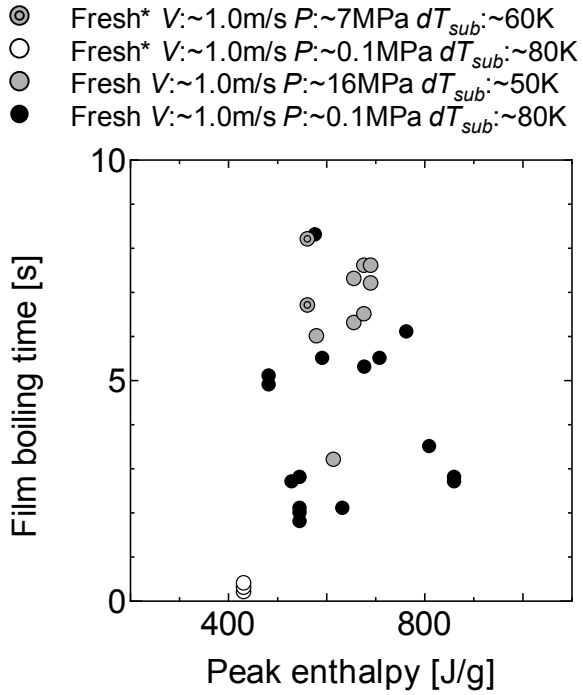

Fig.3.29 Film boiling times for test cases with fresh fuel, coolant flow velocity of ~1.0 m/s, coolant pressures of ~0.1–16 MPa, and coolant subcoolings of ~50–80 K (* : iterative pulse-irradiation experiment)

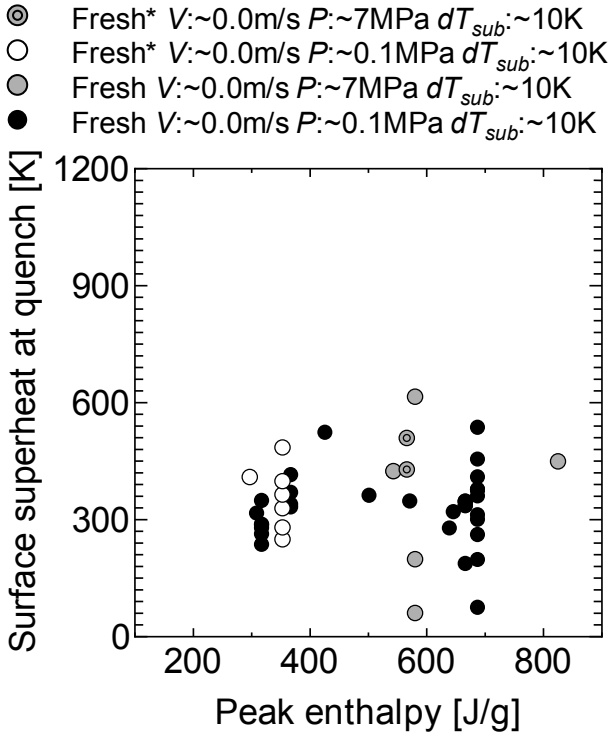

Fig.3.30 Surface superheats at quench for test cases with fresh fuel, stagnant coolant, coolant pressures of ~0.1–7 MPa, and coolant subcoolings of ~10 K (* : iterative pulse-irradiation experiment)

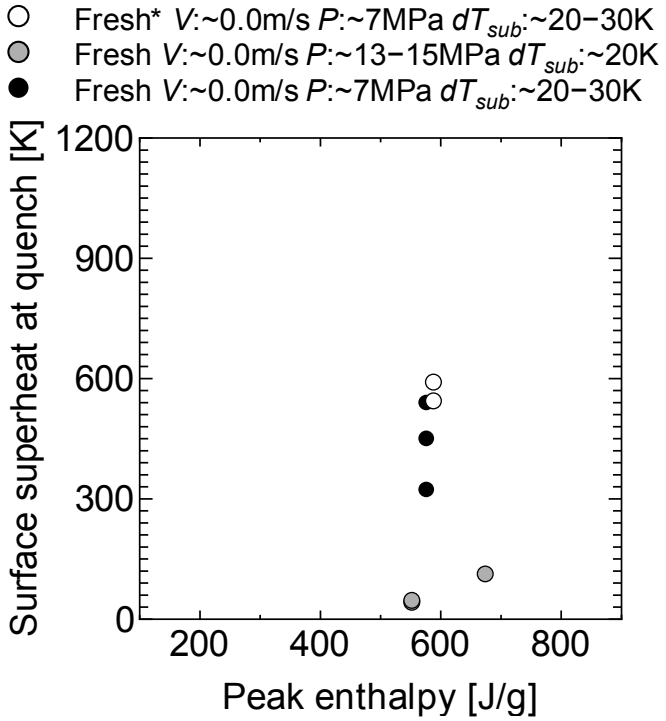

Fig.3.31 Film boiling times for test cases with fresh fuel, stagnant coolant, coolant pressures of ~7–15 MPa, and coolant subcoolings of ~20–30 K (* : iterative pulse-irradiation experiment)

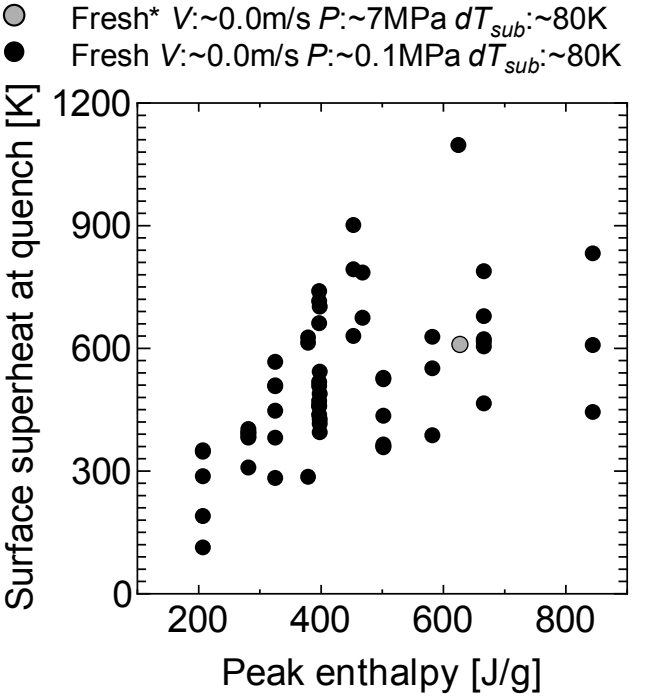

Fig.3.32 Surface superheats at quench for test cases with fresh fuel, stagnant coolant, coolant pressures of ~0.1–7 MPa, and coolant subcooling of ~80 K (* : iterative pulse-irradiation experiment)

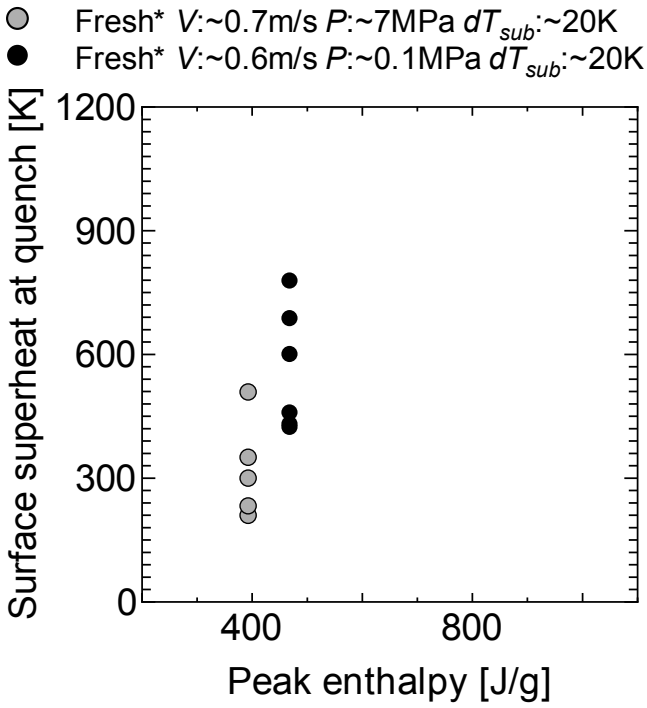

Fig.3.33 Surface superheats at quench for test cases with fresh fuel, coolant flow velocities of ~0.6–0.7 m/s, coolant pressures of ~0.1–7 MPa, and coolant subcooling of ~20 K (* : iterative pulse-irradiation experiment)

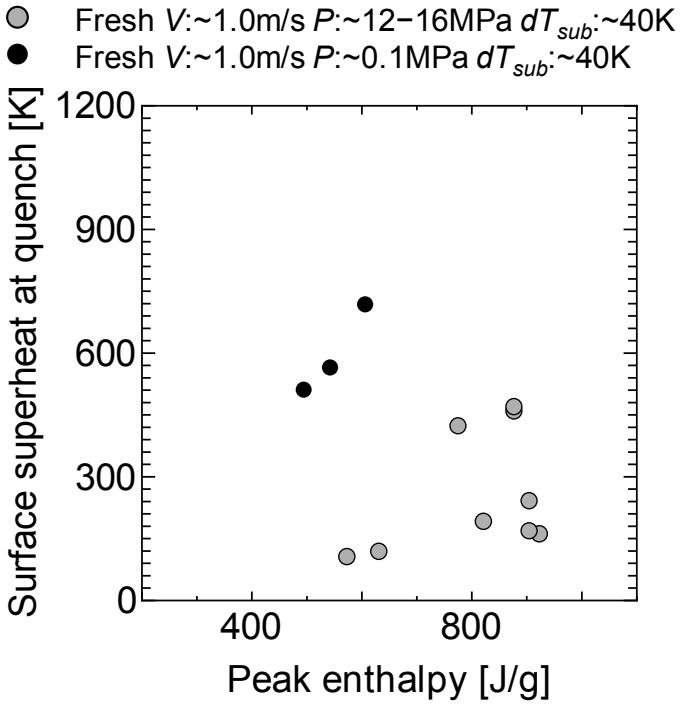

Fig.3.34 Surface superheats at quench for test cases with fresh fuel, coolant flow velocity of ~1.0 m/s, coolant pressures of ~0.1–16 MPa, and coolant subcooling of ~40 K

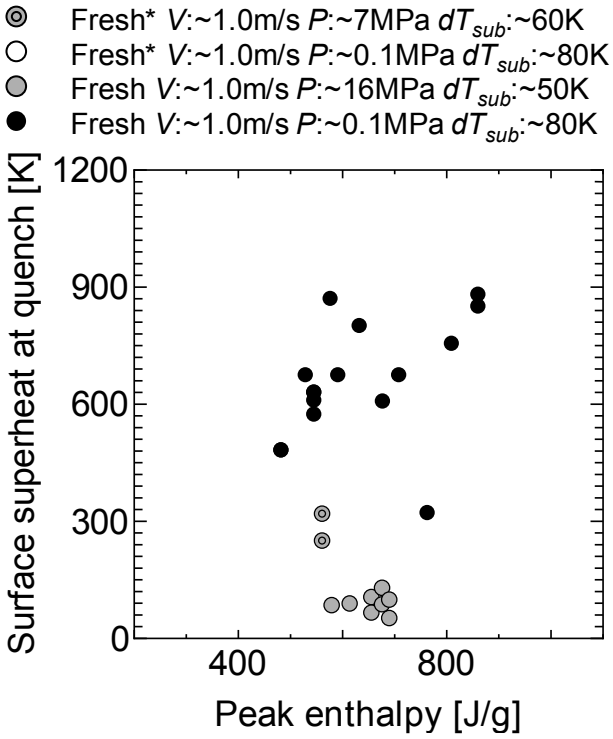

Fig.3.35 Surface superheats at quench for test cases with fresh fuel, coolant flow velocity of ~1.0 m/s, coolant pressures of ~0.1–16 MPa, and coolant subcoolings of ~50–80 K (* : iterative pulse-irradiation experiment)

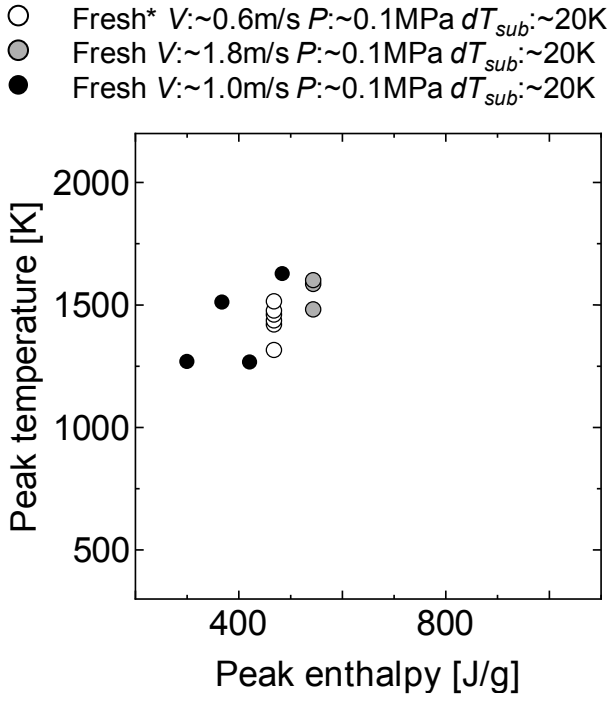

Fig.3.36 Peak temperatures for test cases with fresh fuel, coolant flow velocities of ~0.6–1.8 m/s, atmospheric coolant pressure, and coolant subcooling of ~20 K (* : iterative pulse-irradiation experiment)

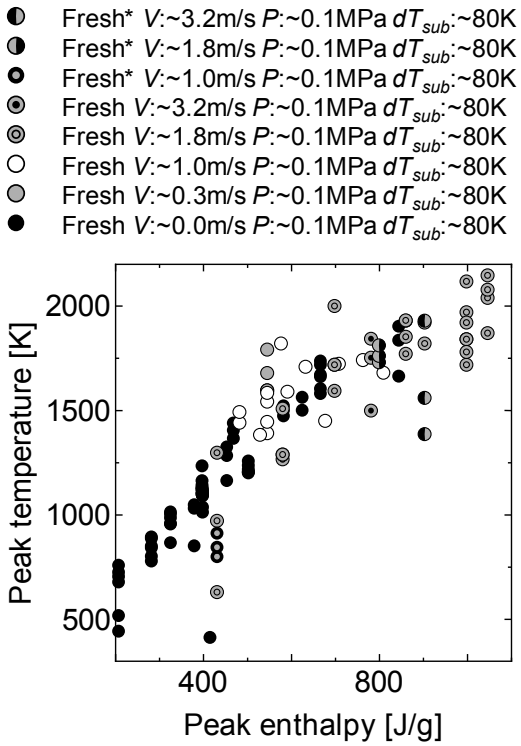

Fig.3.37　Peak temperatures for test cases with fresh fuel, coolant flow velocities of ~0.0–3.2 m/s, atmospheric coolant pressure, and coolant subcooling of ~80 K (* : iterative pulse-irradiation experiment)

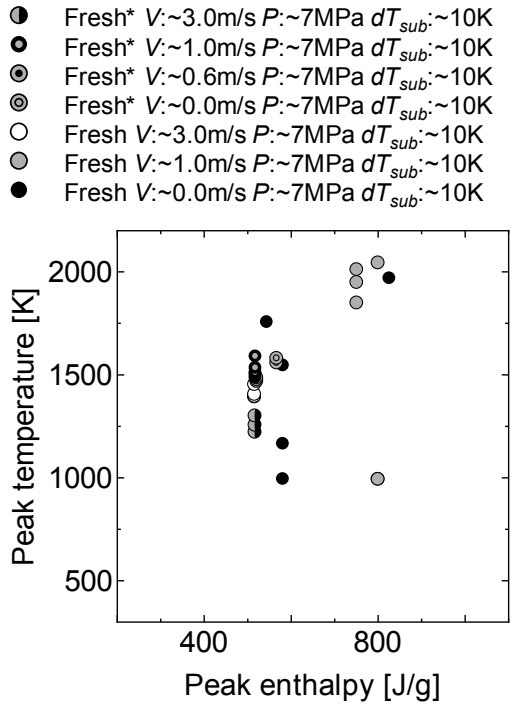

Fig.3.38　Peak temperatures for test cases with fresh fuel, coolant flow velocities of ~0.0–3.0 m/s, coolant pressure of ~7 MPa, and coolant subcooling of ~10 K (* : iterative pulse-irradiation experiment)

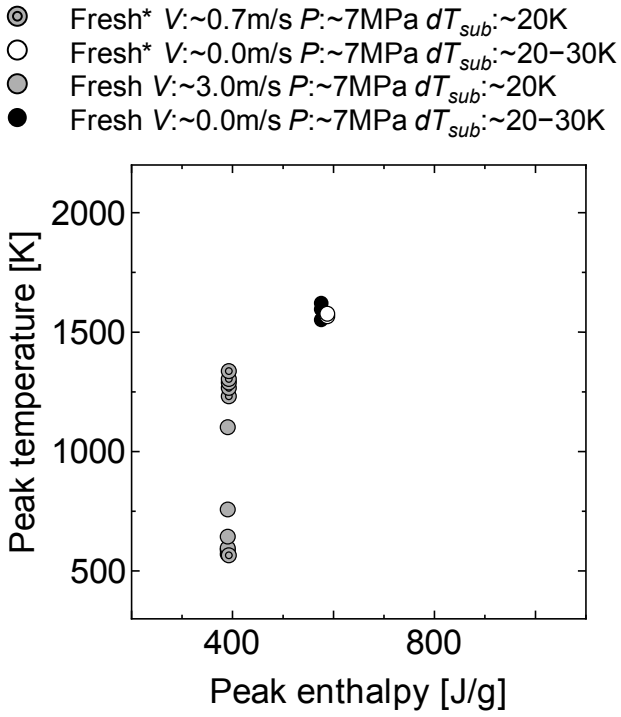

Fig.3.39 Peak temperatures for test cases with fresh fuel, coolant flow velocities of ~0.0–3.0 m/s, coolant pressure of ~7 MPa, and coolant subcoolings of ~10–30 K (* : iterative pulse-irradiation experiment)

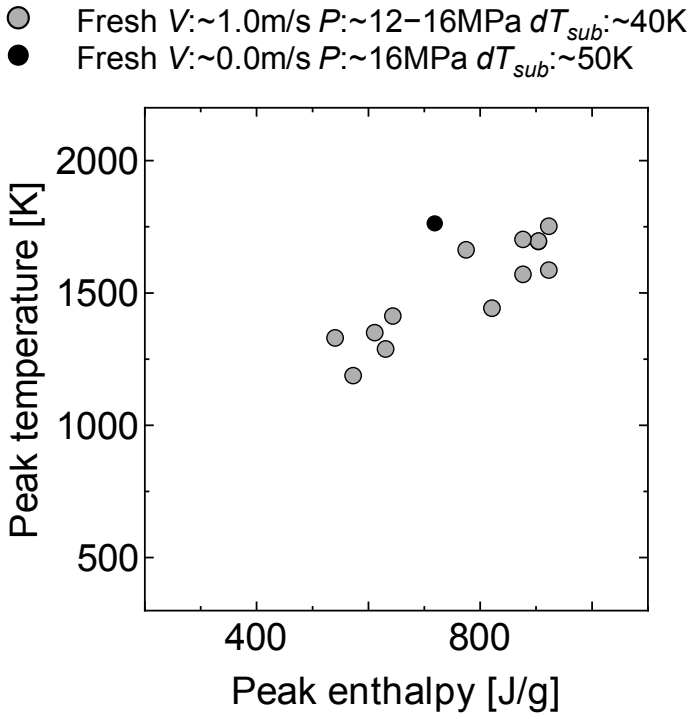

Fig.3.40 Peak temperatures for test cases with fresh fuel, coolant flow velocities of ~0.0–1.0 m/s, coolant pressures of ~12–16 MPa, and coolant subcoolings of ~40–50 K

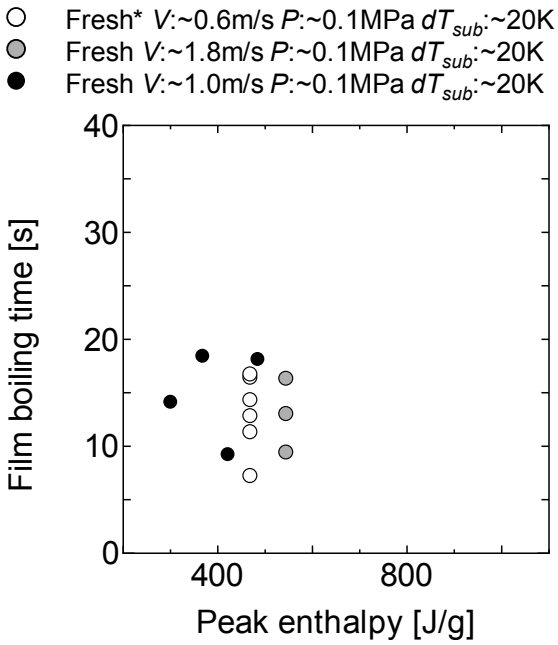

Fig.3.41　Film boiling times for test cases with fresh fuel, coolant flow velocities of ~0.6–1.8 m/s, atmospheric coolant pressure, and coolant subcooling of ~20 K (* : iterative pulse-irradiation experiment)

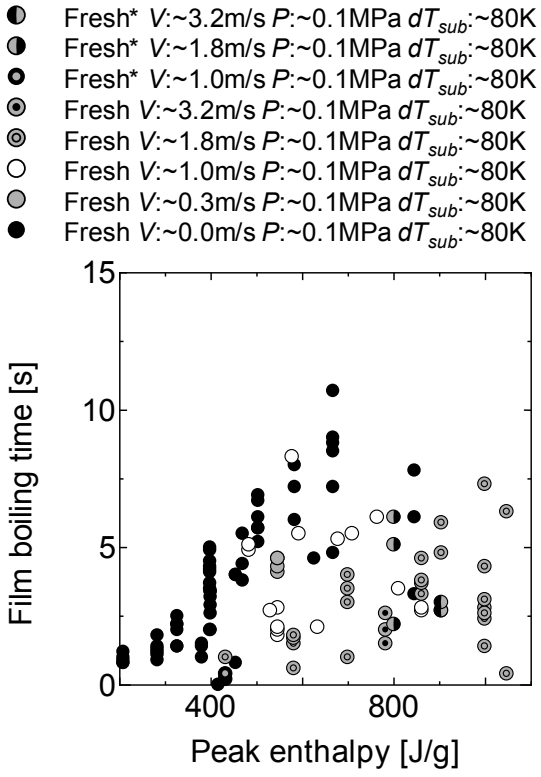

Fig.3.42　Film boiling times for test cases with fresh fuel, coolant flow velocities of ~0.0–3.2 m/s, atmospheric coolant pressure, and coolant subcooling of ~80 K (* : iterative pulse-irradiation experiment)

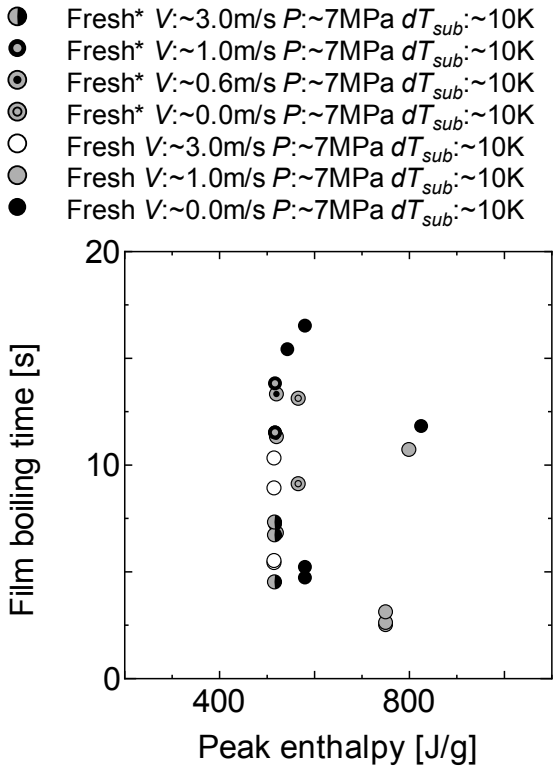

Fig.3.43 Film boiling times for test cases with fresh fuel, coolant flow velocities of ~0.0–3.0 m/s, coolant pressure of ~7 MPa, and coolant subcooling of ~10 K (* : iterative pulse-irradiation experiment)

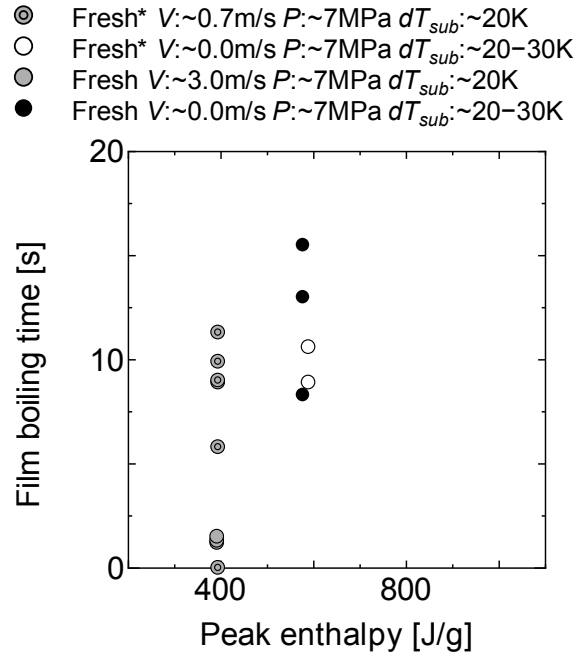

Fig.3.44 Film boiling times for test cases with fresh fuel, coolant flow velocities of ~0.0–3.0 m/s, coolant pressure of ~7 MPa, and coolant subcoolings of ~10–30 K (* : iterative pulse-irradiation experiment)

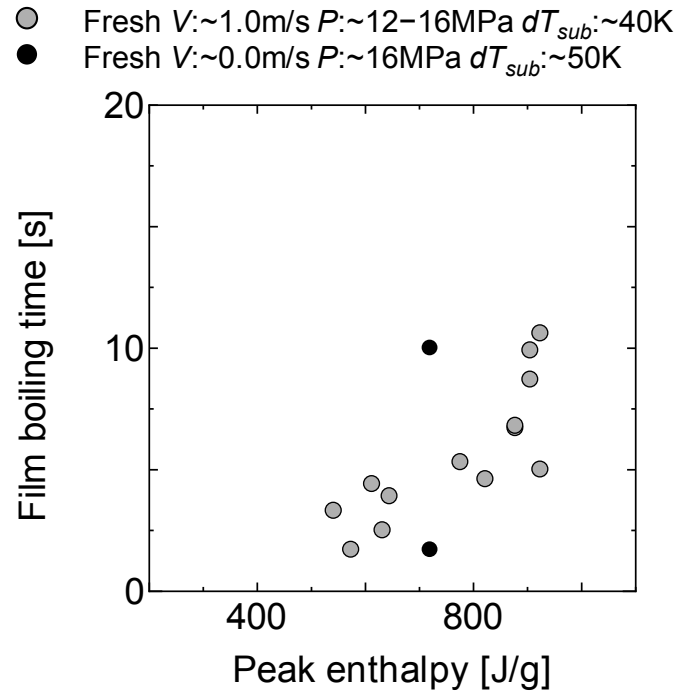

Fig.3.45　Film boiling times for test cases with fresh fuel, coolant flow velocities of ~0.0–1.0 m/s, coolant pressures of ~12–16 MPa, and coolant subcoolings of ~40–50 K

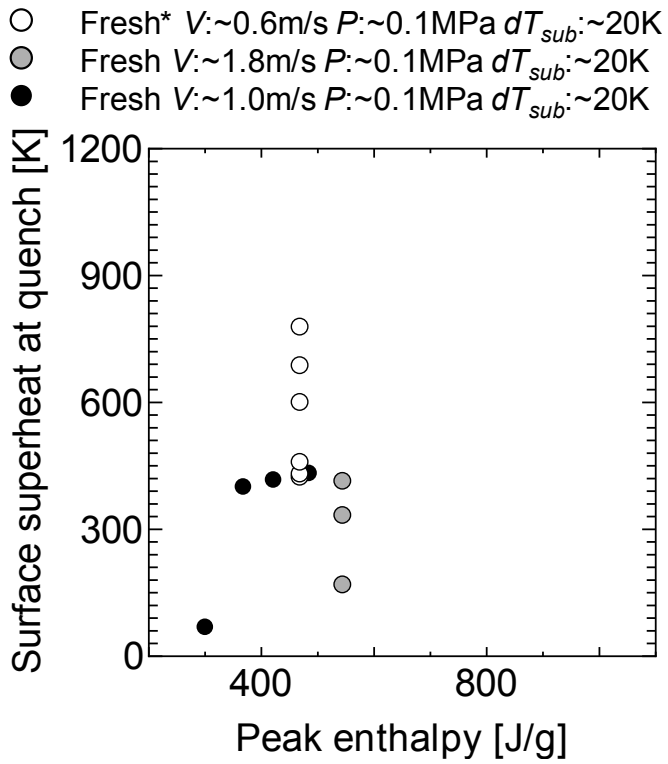

Fig.3.46　Surface superheats at quench for test cases with fresh fuel, coolant flow velocities of ~0.6–1.8 m/s, atmospheric coolant pressure, and coolant subcooling of ~20 K (* : iterative pulse-irradiation experiment)

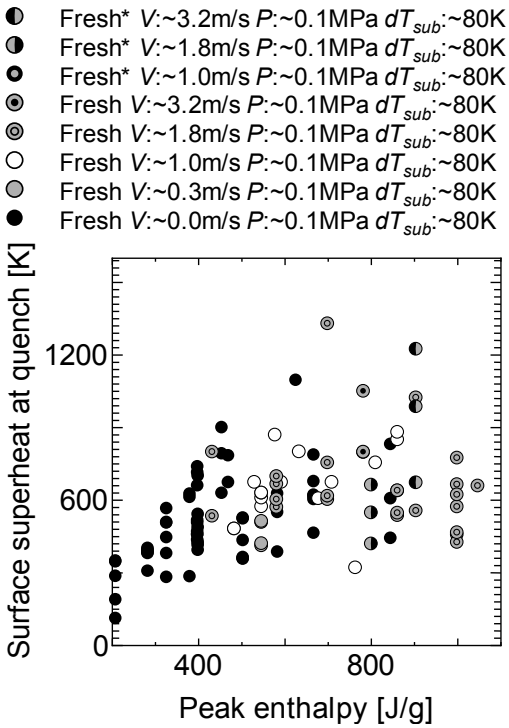

Fig.3.47 Surface superheats at quench for test cases with fresh fuel, coolant flow velocities of ~0.0–3.2 m/s, atmospheric coolant pressure, and coolant subcooling of ~80 K (* : iterative pulse-irradiation experiment)

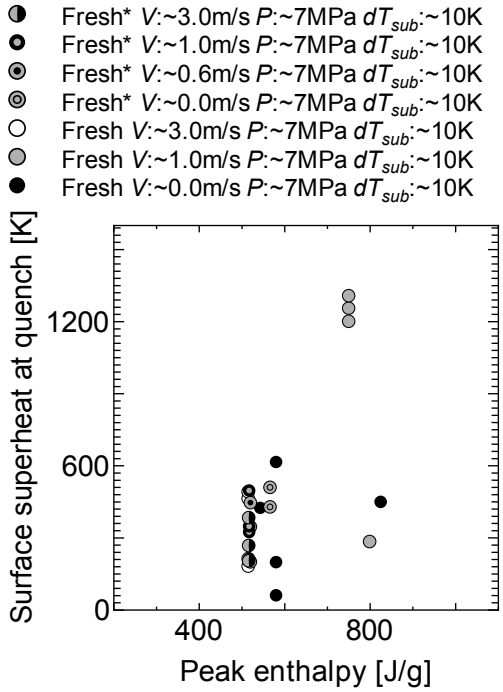

Fig.3.48 Surface superheats at quench for test cases with fresh fuel, coolant flow velocities of ~0.0–3.0 m/s, coolant pressure of ~7 MPa, and coolant subcooling of ~10 K (* : iterative pulse-irradiation experiment)

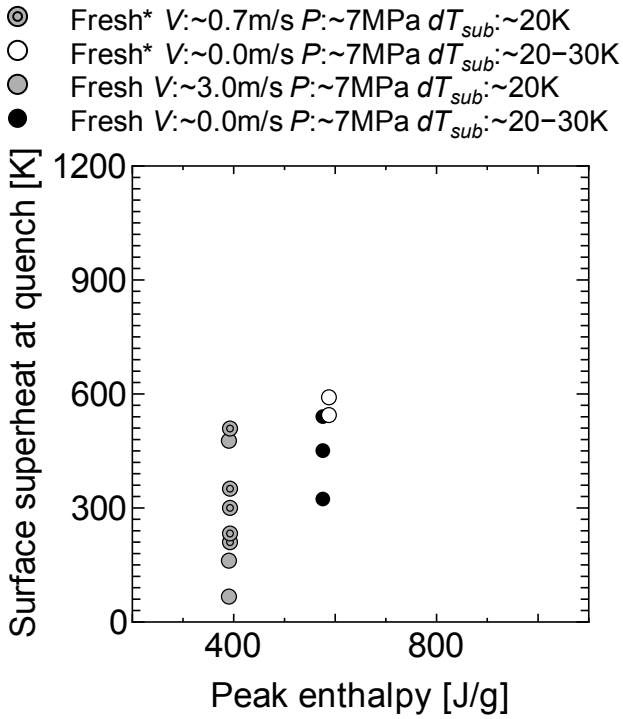

Fig.3.49 Surface superheats at quench for test cases with fresh fuel, coolant flow velocities of ~0.0–3.0 m/s, coolant pressure of ~7 MPa, and coolant subcoolings of ~10–30 K (* : iterative pulse-irradiation experiment)

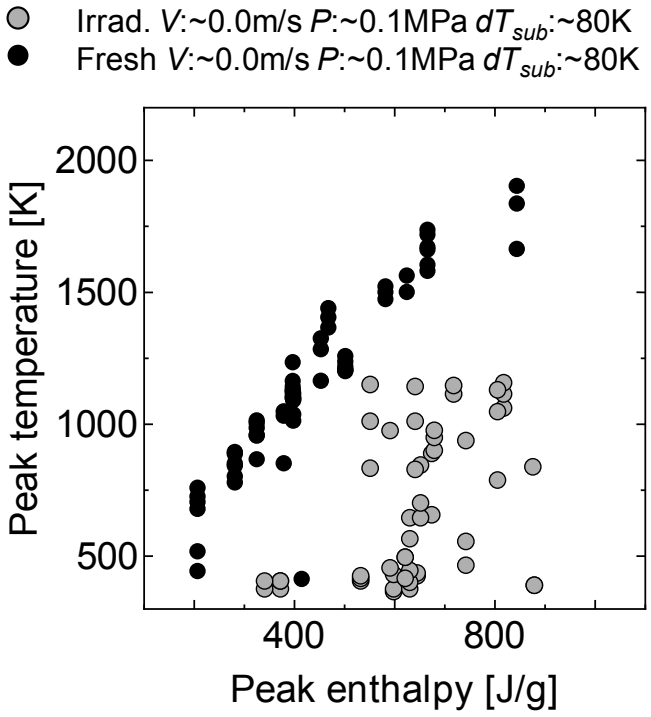

Fig.3.50 Peak temperatures for test cases with fresh and irradiated fuels, stagnant coolant, atmospheric coolant pressure, and coolant subcooling of ~80 K

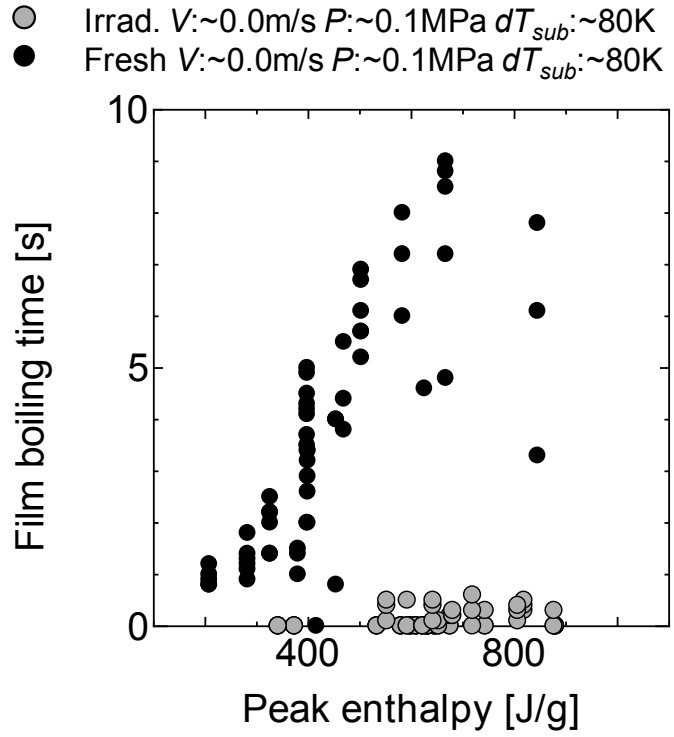

Fig.3.51 Film boiling times for test cases with fresh and irradiated fuels, stagnant coolant, atmospheric coolant pressure, and coolant subcooling of ~80 K

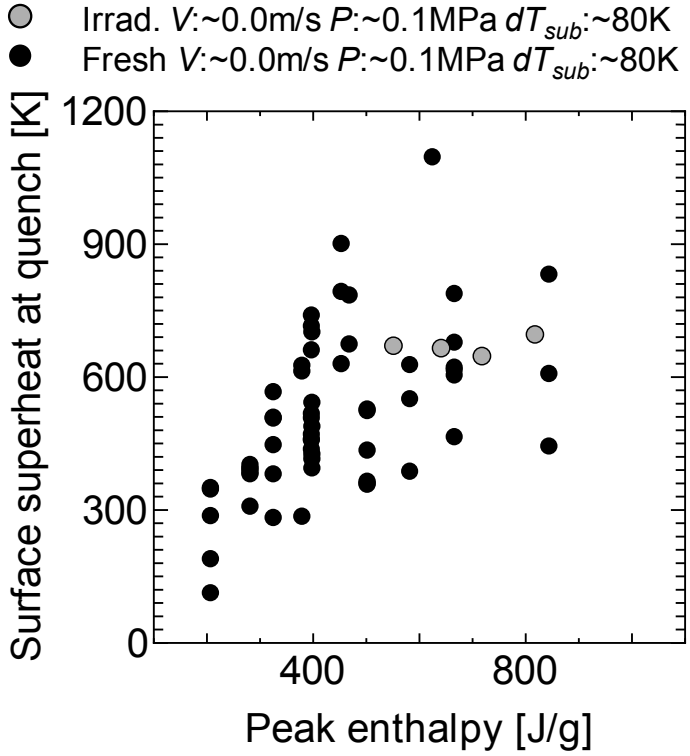

Fig.3.52 Surface superheats at quench for test cases with fresh and irradiated fuels, stagnant coolant, atmospheric coolant pressure, and coolant subcooling of ~80 K

This is a blank page.

国際単位系（SI）

表１．SI 基本単位

基本量	SI 基本単位	
	名称	記号
長さ	メートル	m
質量	キログラム	kg
時間	秒	s
電流	アンペア	A
熱力学温度	ケルビン	K
物質量	モル	mol
光度	カンデラ	cd

表２．基本単位を用いて表されるSI組立単位の例

組立量	SI 基本単位	
	名称	記号
面積	平方メートル	m^2
体積	立法メートル	m^3
速さ，速度	メートル毎秒	m/s
加速度	メートル毎秒毎秒	m/s^2
波数	毎メートル	m^{-1}
密度，質量密度	キログラム毎立方メートル	kg/m^3
面積密度	キログラム毎平方メートル	kg/m^2
比体積	立方メートル毎キログラム	m^3/kg
電流密度	アンペア毎平方メートル	A/m^2
磁界の強さ	アンペア毎メートル	A/m
量濃度(a)，濃度	モル毎立方メートル	mol/m^3
質量濃度	キログラム毎立法メートル	kg/m^3
輝度	カンデラ毎平方メートル	cd/m^2
屈折率(b)	（数字の） 1	1
比透磁率(b)	（数字の） 1	1

(a) 量濃度（amount concentration）は臨床化学の分野では物質濃度（substance concentration）ともよばれる。
(b) これらは無次元量あるいは次元１をもつ量であるが、そのことを表す単位記号である数字の１は通常は表記しない。

表３．固有の名称と記号で表されるSI組立単位

組立量	SI 組立単位			
	名称	記号	他のSI単位による表し方	SI基本単位による表し方
平面角	ラジアン(b)	rad	1 (b)	m/m
立体角	ステラジアン(b)	sr(c)	1 (b)	m^2/m^2
周波数	ヘルツ(d)	Hz		s^{-1}
力	ニュートン	N		m kg s^{-2}
圧力，応力	パスカル	Pa	N/m^2	m^{-1} kg s^{-2}
エネルギー，仕事，熱量	ジュール	J	N m	m^2 kg s^{-2}
仕事率，工率，放射束	ワット	W	J/s	m^2 kg s^{-3}
電荷，電気量	クーロン	C		s A
電位差（電圧），起電力	ボルト	V	W/A	m^2 kg s^{-3} A^{-1}
静電容量	ファラド	F	C/V	m^{-2} kg^{-1} s^4 A^2
電気抵抗	オーム	Ω	V/A	m^2 kg s^{-3} A^{-2}
コンダクタンス	ジーメンス	S	A/V	m^{-2} kg^{-1} s^3 A^2
磁束	ウエーバ	Wb	Vs	m^2 kg s^{-2} A^{-1}
磁束密度	テスラ	T	Wb/m^2	kg s^{-2} A^{-1}
インダクタンス	ヘンリー	H	Wb/A	m^2 kg s^{-2} A^{-2}
セルシウス温度	セルシウス度(e)	℃		K
光束	ルーメン	lm	cd sr(c)	cd
照度	ルクス	lx	lm/m^2	m^{-2} cd
放射性核種の放射能(f)	ベクレル(d)	Bq		s^{-1}
吸収線量, 比エネルギー分与, カーマ	グレイ	Gy	J/kg	m^2 s^{-2}
線量当量, 周辺線量当量, 方向性線量当量, 個人線量当量	シーベルト(g)	Sv	J/kg	m^2 s^{-2}
酸素活性	カタール	kat		s^{-1} mol

(a)SI接頭語は固有の名称と記号を持つ組立単位と組み合わせても使用できる。しかし接頭語を付した単位はもはやコヒーレントではない。
(b)ラジアンとステラジアンは数字の１に対する単位の特別な名称で、量についての情報をつたえるために使われる。実際には、使用する時には記号radおよびsrが用いられるが、習慣として組立単位としての記号である数字の１は明示されない。
(c)測光学ではステラジアンという名称と記号srを単位の表し方の中に、そのまま維持している。
(d)ヘルツは周期現象についてのみ、ベクレルは放射性核種の統計的過程についてのみ使用される。
(e)セルシウス度はケルビンの特別な名称で、セルシウス温度を表すために使用される。セルシウス度とケルビンの単位の大きさは同一である。したがって、温度差や温度間隔を表す数値はどちらの単位で表しても同じである。
(f)放射性核種の放射能（activity referred to a radionuclide）は、しばしば誤った用語で"radioactivity"と記される。
(g)単位シーベルト（PV,2002,70,205）についてはCIPM勧告2（CI-2002）を参照。

表４．単位の中に固有の名称と記号を含むSI組立単位の例

組立量	SI 組立単位		
	名称	記号	SI 基本単位による表し方
粘度	パスカル秒	Pa s	m^{-1} kg s^{-1}
力のモーメント	ニュートンメートル	N m	m^2 kg s^{-2}
表面張力	ニュートン毎メートル	N/m	kg s^{-2}
角速度	ラジアン毎秒	rad/s	m m^{-1} s^{-1}=s^{-1}
角加速度	ラジアン毎秒毎秒	rad/s^2	m m^{-1} s^{-2}=s^{-2}
熱流密度，放射照度	ワット毎平方メートル	W/m^2	kg s^{-3}
熱容量，エントロピー	ジュール毎ケルビン	J/K	m^2 kg s^{-2} K^{-1}
比熱容量，比エントロピー	ジュール毎キログラム毎ケルビン	J/(kg K)	m^2 s^{-2} K^{-1}
比エネルギー	ジュール毎キログラム	J/kg	m^2 s^{-2}
熱伝導率	ワット毎メートル毎ケルビン	W/(m K)	m kg s^{-3} K^{-1}
体積エネルギー	ジュール毎立方メートル	J/m^3	m^{-1} kg s^{-2}
電界の強さ	ボルト毎メートル	V/m	m kg s^{-3} A^{-1}
電荷密度	クーロン毎立方メートル	C/m^3	m^{-3} sA
表面電荷	クーロン毎平方メートル	C/m^2	m^{-2} sA
電束密度，電気変位	クーロン毎平方メートル	C/m^2	m^{-2} sA
誘電率	ファラド毎メートル	F/m	m^{-3} kg^{-1} s^4 A^2
透磁率	ヘンリー毎メートル	H/m	m kg s^{-2} A^{-2}
モルエネルギー	ジュール毎モル	J/mol	m^2 kg s^{-2} mol^{-1}
モルエントロピー, モル熱容量	ジュール毎モル毎ケルビン	J/(mol K)	m^2 kg s^{-2} K^{-1} mol^{-1}
照射線量（X線及びγ線）	クーロン毎キログラム	C/kg	kg^{-1} sA
吸収線量率	グレイ毎秒	Gy/s	m^2 s^{-3}
放射強度	ワット毎ステラジアン	W/sr	m^4 m^{-2} kg s^{-3}=m^2 kg s^{-3}
放射輝度	ワット毎平方メートル毎ステラジアン	$W/(m^2$ sr)	m^2 m^{-2} kg s^{-3}=kg s^{-3}
酵素活性濃度	カタール毎立方メートル	kat/m^3	m^{-3} s^{-1} mol

表５．SI 接頭語

乗数	接頭語	記号	乗数	接頭語	記号
10^{24}	ヨタ	Y	10^{-1}	デシ	d
10^{21}	ゼタ	Z	10^{-2}	センチ	c
10^{18}	エクサ	E	10^{-3}	ミリ	m
10^{15}	ペタ	P	10^{-6}	マイクロ	μ
10^{12}	テラ	T	10^{-9}	ナノ	n
10^9	ギガ	G	10^{-12}	ピコ	p
10^6	メガ	M	10^{-15}	フェムト	f
10^3	キロ	k	10^{-18}	アト	a
10^2	ヘクト	h	10^{-21}	ゼプト	z
10^1	デカ	da	10^{-24}	ヨクト	y

表６．SIに属さないが、SIと併用される単位

名称	記号	SI 単位による値
分	min	1 min=60s
時	h	1h =60 min=3600 s
日	d	1 d=24 h=86 400 s
度	°	1°=(π/180) rad
分	’	1’=(1/60)°=(π/10800) rad
秒	”	1”=(1/60)’=(π/648000) rad
ヘクタール	ha	$1ha=1hm^2=10^4m^2$
リットル	L, l	$1L=11=1dm^3=10^3cm^3=10^{-3}m^3$
トン	t	$1t=10^3$ kg

表７．SIに属さないが、SIと併用される単位で、SI単位で表される数値が実験的に得られるもの

名称	記号	SI 単位で表される数値
電子ボルト	eV	$1eV=1.602\ 176\ 53(14)\times10^{-19}J$
ダルトン	Da	$1Da=1.660\ 538\ 86(28)\times10^{-27}kg$
統一原子質量単位	u	1u=1 Da
天文単位	ua	$1ua=1.495\ 978\ 706\ 91(6)\times10^{11}m$

表８．SIに属さないが、SIと併用されるその他の単位

名称	記号	SI 単位で表される数値
バール	bar	1 bar=0.1MPa=100kPa=10^5Pa
水銀柱ミリメートル	mmHg	1mmHg=133.322Pa
オングストローム	Å	1 Å=0.1nm=100pm=10^{-10}m
海里	M	1 M=1852m
バーン	b	$1\ b=100fm^2=(10^{-12}cm)2=10^{-28}m^2$
ノット	kn	1 kn=(1852/3600)m/s
ネーパ	Np	SI単位との数値的な関係は、対数量の定義に依存。
ベル	B	
デジベル	dB	

表９．固有の名称をもつCGS組立単位

名称	記号	SI 単位で表される数値
エルグ	erg	$1\ erg=10^{-7}$ J
ダイン	dyn	$1\ dyn=10^{-5}$N
ポアズ	P	1 P=1 dyn s cm^{-2}=0.1Pa s
ストークス	St	1 St =$1cm^2$ s^{-1}=$10^{-4}m^2$ s^{-1}
スチルブ	sb	1 sb =1cd cm^{-2}=10^4cd m^{-2}
フォト	ph	1 ph=1cd sr cm^{-2} 10^4lx
ガル	Gal	1 Gal =1cm s^{-2}=$10^{-2}ms^{-2}$
マクスウェル	Mx	1 Mx = 1G cm^2=10^{-8}Wb
ガウス	G	1 G =1Mx cm^{-2} =10^{-4}T
エルステッド(c)	Oe	1 Oe≙ $(10^3/4\pi)$A m^{-1}

(c) ３元系のCGS単位系とSIでは直接比較できないため、等号「 ≙ 」は対応関係を示すものである。

表10．SIに属さないその他の単位の例

名称	記号	SI 単位で表される数値
キュリー	Ci	$1\ Ci=3.7\times10^{10}Bq$
レントゲン	R	$1\ R = 2.58\times10^{-4}C/kg$
ラド	rad	$1\ rad=1cGy=10^{-2}Gy$
レム	rem	$1\ rem=1\ cSv=10^{-2}Sv$
ガンマ	γ	1γ=1 nT=10-9T
フェルミ		1フェルミ=1 fm=10-15m
メートル系カラット		1メートル系カラット = 200 mg = 2×10-4kg
トル	Torr	1 Torr = (101 325/760) Pa
標準大気圧	atm	1 atm = 101 325 Pa
カロリー	cal	1cal=4.1858J（「15℃」カロリー），4.1868J（「IT」カロリー）4.184J（「熱化学」カロリー）
ミクロン	μ	1 μ =1μm=10^{-6}m

（第8版，2006年改訂）

この印刷物は再生紙を使用しています